

**DEGRADATION OF A BI-FACIAL SOLAR PANEL UNDER THE SUN**

**ANG CHONG HUAH**

**A project report submitted in partial fulfilment of the  
requirements for the award of Bachelor of Engineering  
(Hons.) Mechanical Engineering**

**Lee Kong Chian Faculty of Engineering and Science  
Universiti Tunku Abdul Rahman**

**May 2015**

## DECLARATION

I hereby declare that this project report is based on my original work except for citations and quotations which have been duly acknowledged. I also declare that it has not been previously and concurrently submitted for any other degree or award at UTAR or other institutions.

Signature : \_\_\_\_\_

Name : ANG CHONG HUAH

ID No. : 10UEB05732

Date : 4/5/2015

**APPROVAL FOR SUBMISSION**

I certify that this project report entitled **“DEGRADATION OF A BI-FACIAL SOLAR PANEL UNDER THE SUN”** was prepared by **ANG CHONG HUAH** has met the required standard for submission in partial fulfilment of the requirements for the award of Bachelor of Engineering (Hons.) Mechanical Engineering at Universiti Tunku Abdul Rahman.

Approved by,

Signature : \_\_\_\_\_

Supervisor : **DR KAREN WONG MEE CHU**  
\_\_\_\_\_

Date : **4/5/2015**  
\_\_\_\_\_

The copyright of this report belongs to the author under the terms of the copyright Act 1987 as qualified by Intellectual Property Policy of Universiti Tunku Abdul Rahman. Due acknowledgement shall always be made of the use of any material contained in, or derived from, this report.

© 2015, Ang Chong Huah. All right reserved.

## ACKNOWLEDGEMENTS

First of all, I owe my deepest gratitude to University Tunku Abdul Rahman (UTAR) for providing all the facilities and equipments for me to complete my Final Year Project as a partial fulfilment of the requirement for my Bachelor Degree Programme in Mechanical Engineering.

Throughout this project, I'm indebted to my supervisor, Dr Karen Wong Mee Chu, for her technical advice, guidance, encouragement and support. I also wish to take this opportunity to thank Prof. Dr Lim Yun Seng from Department of Electrical and Electronic Engineering for his helpful suggestions.

In addition, a special thanks to my senior Mr Lo Chin Kim who is currently PhD student. Without his constant help and guidance, this project would not have been possible.

I would also like to express my appreciation to the lab officers who aided me during my project.

Last but not least, I would like to thank to my parents and fellow friends for their encouragement and support.

## DEGRADATION OF A BI-FACIAL SOLAR PANEL UNDER THE SUN

### ABSTRACT

Bi-facial solar cells are able to produce 30% more solar electricity compared to conventional solar cells. In this project, Platinum (Pt)-reinforced Sn-3.0Ag-0.5Cu (SAC) solder was used as interconnection material in bi-facial solar cells. Pt was used as reinforcement as it is expected to increase conductivity of the solar panel and reduce excessive growth of intermetallic compound (IMC) layer in the solar ribbon-solder-solar cell sandwich structure. Two sets of samples were prepared, one with 0.40 wt.% Pt inclusion and the other without. These samples were exposed under the sunlight for a duration of up to five weeks. An additional set of samples were heat-treated at 80°C for up to 48 hours to study the effect of accelerated aging on the solar cells. All samples were prepared for metallographic examination before imaging using optical and scanning electron microscope (SEM). The IMC layer was identified using Energy-dispersive X-ray (EDX) spectroscopy analysis. It was found that the IMC layer decreased 19.43% when 0.40 wt.% Pt was added to the solder even after five weeks of exposure under the sunlight. It was observed that there are noticeably less Kirkendall voids and micro-cracks in the Pt-containing samples. This observation is supported by the resistivity results, whereby samples containing Pt have resistivity of about 77% lower than that without Pt inclusions. It is believed that Pt shows the diffusion rate of other species in the solar cell sandwich structure, thus reducing the IMC layer thickness and also presence of Kirkendall voids and micro-cracks. As a result of a less disordered structure, the electrical conductivity of the solar panel is improved via inclusions of Pt particles to the SAC solder in the bi-facial solar panel.

## TABLE OF CONTENTS

<b>DECLARATION</b>	<b>ii</b>
<b>APPROVAL FOR SUBMISSION</b>	<b>iii</b>
<b>ACKNOWLEDGEMENTS</b>	<b>v</b>
<b>ABSTRACT</b>	<b>vi</b>
<b>TABLE OF CONTENTS</b>	<b>vii</b>
<b>LIST OF TABLES</b>	<b>ix</b>
<b>LIST OF FIGURES</b>	<b>xi</b>
<b>LIST OF SYMBOLS / ABBREVIATIONS</b>	<b>xv</b>
<b>LIST OF APPENDICES</b>	<b>xvi</b>

### CHAPTER

<b>1</b>	<b>INTRODUCTION</b>	<b>1</b>
	1.1 Background	1
	1.2 Aims and Objectives	2
<b>2</b>	<b>LITERATURE REVIEW</b>	<b>4</b>
	2.1 Solar Cells	4
	2.1.1 Types of Solar Cells	4
	2.1.2 Advantages and Disadvantages of Solar Energy	6
	2.2 Bi-facial Solar Cells	7
	2.2.1 Fundamentals of Bi-facial Solar Cells	7
	2.3 Degradation of Solar Modules	8
	2.4 Lead-Free Solders	10
	2.5 Intermetallic Reaction and Growth of Solder Paste with Pt	11
	2.6 Addition of Different Elements to Solder Paste	13

2.7	Reflow Soldering	14
2.7.1	Reflow Specification	14
<b>3</b>	<b>METHODOLOGY</b>	<b>17</b>
3.1	Materials and Methods	17
3.1.1	EarthON Bi-facial Solar Cells	17
3.1.2	Lead Coated Ribbon	20
3.1.3	Solder	21
3.1.4	Rosin Mildly Activated (RMA) Flux	21
3.1.5	Weifo Microprocessor Controlled Programmable Oven	22
3.2	Inclusion of Platinum into Solder Paste	22
3.3	Pre-Soldering Preparation	22
3.4	Bi-facial Solar Cell Soldering	24
3.5	Encapsulation Process	26
3.6	Solar Cell Microstructure Study Preparation	27
3.7	Specimen Preparation	28
3.7.1	Resistivity Measurements for Solder Contact	28
<b>4</b>	<b>RESULTS AND DISCUSSION</b>	<b>33</b>
4.1	Microstructure of SAC and SAC-0.40Pt Solder Solar Sandwich Structure	33
4.2	Microstructure of Samples after Exposure Under the Sun	43
4.3	Microstructure of Samples after Heat Treatment	52
4.4	Resistivity of Samples after Heat Treatment	58
<b>5</b>	<b>CONCLUSION AND RECOMMENDATIONS</b>	<b>66</b>
5.1	Conclusion	66
5.2	Recommendations	67
	<b>REFERENCES</b>	<b>68</b>
	<b>APPENDICES</b>	<b>71</b>

## LIST OF TABLES

TABLE	TITLE	PAGE
3.1	Recommended Soldering Condition for EarthON Bi-facial Solar Cell	19
4.1	IMC Thickness of the $\text{Cu}_6\text{Sn}_5$ Layer Formed at the SAC Solder-Ribbon Interface	41
4.2	IMC Thickness of the $\text{Cu}_6\text{Sn}_5$ Layer Formed at the SAC-0.40Pt Solder-Ribbon Interface	42
4.3	IMC Thickness of the $\text{Cu}_6\text{Sn}_5$ Layer Formed at the SAC Solder-Ribbon Interface (Week 1)	46
4.4	IMC Thickness of the $\text{Cu}_6\text{Sn}_5$ Layer Formed at the SAC-0.40Pt Solder-Ribbon Interface (Week 1)	47
4.5	IMC Layer Thickness for SAC and SAC-0.40Pt Solder Solar Cells at Different Weeks	49
4.6	IMC Layer Thickness for SAC and SAC-0.40Pt Solder Solar Cells for Different Heat Treatment Times	55
4.7	Resistance Value for Each Point on the Bi-facial Solar Cell (Without Heat Treatment)	58
4.8	Resistance Value for Each Point on the Bi-facial Solar Cell (Without Heat Treatment)	59
4.9	Summary of $R_{busbar}$ and $R_c$ for SAC Solder Solar Cells before and after Heat Treatment for Different Duration	61
4.10	Summary of $R_{busbar}$ and $R_c$ for SAC-0.40Pt Solder Solar Cells before and after Heat Treatment for Different Duration	61
4.11	Specific Solder Contact Resistivity for SAC Solder Solar Cells before and after Different Heat Treatment Duration	62

4.12	Specific Solder Contact Resistivity for SAC-0.40Pt Solder Solar Cells before and after Different Heat Treatment Duration	62
4.13	Percentage Difference for Specific Solder Contact Resistivity for SAC Solder Solar Cells after Different Heat Treatment Duration	63
4.14	Percentage Difference for Specific Solder Contact Resistivity for SAC-0.40Pt Solder Solar Cells after Different Heat Treatment Duration	64

## LIST OF FIGURES

FIGURE	TITLE	PAGE
2.1	Leakage Current and Voltage Potential (negative potential shown) Cause Negative (-) Ions to Migrate Away from the Semiconductor, as Positive (+) Ions Migrate Toward the Semiconductor from the Glass and Package, and the Module's External Environment (Advanced Energy, 2013)	8
2.2	Base Resistivity Dependence of PID (Pingel, S., 2009)	9
2.3	The Intermetallic Microstructure of Sn-3.8Ag-0.7Cu Solder after Reflow at (a) 30 s, (b) 90 s, (c) 360 s, and (d) 600 s (Kim & Kim, 2004)	12
2.4	Reflow Profile for Lead Free Solder Paste (RedRing Solder, 2013)	15
3.1	EarthON Bi-facial Solar Cell	17
3.2	Cross Section of p-n-n <sup>+</sup> Bi-facial Solar Cell (PVG Solutions Inc, 2011)	18
3.3	EarthON Bi-facial Solar Cell	18
3.4	Dimension of EarthON Bi-facial Solar Cell	19
3.5	Spectral Response Data	20
3.6	Luvata Sunwire of Lead Coated Copper Ribbon	20
3.7	RedRing Solder Paste	21
3.8	Sample of Custom Made Paper Stencil	23
3.9	Sample of Custom Made Paper Stencil for Resistivity Test	24
3.10	Reflow Temperature Profile (Weifo, 2013)	25

3.11	Soldered Bi-facial Solar Cell	25
3.12	Schematic of the Encapsulation Process	26
3.13	Soldered Joint from the Solar Cell	27
3.14	Custom Made Paper Stencil for Resistivity Test and Points Use to Measure the Resistivity of Bi-facial Solar Cells	29
3.15	Electrical Circuit Use to Measure Resistivity of the Bi-facial Solar Cells after Heat Treatment	30
3.16	Illustration of the Solder Joints Resistance Measurement Procedure	31
4.1	Optical Micrograph for (A) SAC and (B) SAC-0.40Pt Solder Solar Sandwich	33
4.2	EDX Spectroscopy Spectrums and Elemental Composition Analysis for the IMC Layer Formed between the Interface of SAC Solder and the Pb Coated Cu Ribbon	35
4.3	EDX Spectroscopy Spectrums and Elemental Composition Analysis for the IMC Layer Formed between the Interface of SAC Solder and the Ag Busbar of Bi-facial Solar Cell	36
4.4	EDX Spectroscopy Spectrums and Elemental Composition Analysis for the IMC Layer Formed between the Interface of SAC-0.40Pt Solder and the Pb Coated Cu Ribbon	37
4.5	EDX Spectroscopy Spectrums and Elemental Composition Analysis for the IMC Formed between the Interface of SAC-0.40Pt Solder and the Ag Busbar of Bi-facial Solar Cell	38
4.6	EDX Spectroscopy Spectrums and Elemental Composition Analysis for the Pb Element on the Solder Paste Region	39
4.7	SEM Micrographs at Solder-Ribbon Interface of Solar Sandwich	40
4.8	IMC Thickness Measurements of the $\text{Cu}_6\text{Sn}_5$ Layer Formed at the SAC Solder-Ribbon Interface	40

4.9	IMC Thickness Measurements of the $\text{Cu}_6\text{Sn}_5$ Layer Formed at the SAC-0.40Pt Solder-Ribbon Interface	41
4.10	SEM Micrographs at Solder-Ag Busbar Interface of Solar Sandwich	43
4.11	SEM Micrographs at the Solder-Ribbon Interface for SAC Solder for Different Weeks	44
4.12	SEM Micrographs at the Solder-Ribbon Interface for SAC-0.40Pt Solder for Different Weeks	45
4.13	IMC Thickness Measurements of the $\text{Cu}_6\text{Sn}_5$ Layer Formed at the SAC Solder-Ribbon Interface (Week1)	46
4.14	IMC Thickness Measurements of the $\text{Cu}_6\text{Sn}_5$ Layer Formed at the SAC-0.40Pt Solder-Ribbon Interface (Week 1)	47
4.15	$\text{Cu}_6\text{Sn}_5$ IMC Layer Thickness for SAC and SAC-0.40Pt Solder Solar Cells at Different Weeks	49
4.16	SEM Micrographs at the Solder-Ag Busbar Interface for SAC Solder	50
4.17	SEM Micrographs at the Solder-Ag Busbar Interface for SAC-0.40Pt Solder	51
4.18	SEM Micrographs at the Solder-Ribbon Interface for SAC Solder after Different Periods of Heat Treatment	53
4.19	SEM Micrographs at the Solder-Ribbon Interface for SAC-0.40Pt Solder after Different Periods of Heat Treatment	54
4.20	$\text{Cu}_6\text{Sn}_5$ IMC layer Thickness for SAC and SAC-0.40Pt Solder for Different Heat Treatment Times	55
4.21	SEM Micrographs at the Solder-Ag Busbar Interface for SAC Solder after Different Periods of Heat Treatment	56
4.22	SEM Micrographs at the Solder-Ag Busbar Interface for SAC-0.40Pt Solder after Different Periods of Heat Treatment	57

4.23	Graph of Total Contact Resistance ( $\Omega$ ) against Distance between Two Solder Joints	60
4.24	Graph of Percentage Difference for Specific Solder Contact Resistivity (%) Versus Different Heat Treatment Duration (Hours)	65

**LIST OF SYMBOLS / ABBREVIATIONS**

<i>wt. %</i>	weight percent
<i>cm</i>	centimetre
$\rho$	resistivity
$P_m$	maximum power, W/m <sup>2</sup>
<i>mm</i>	millimetre
$\mu m$	micrometre
°C	degree celcius
<i>V</i>	voltage (mV)
<i>I</i>	current (mA)
<i>R</i>	resistance ( $\Omega$ )
<i>d</i>	distance
<i>w</i>	width
<i>L</i>	length

**LIST OF APPENDICES**

<b>APPENDIX</b>	<b>TITLE</b>	<b>PAGE</b>
A	Resistivity Test Data	71

## **CHAPTER 1**

### **INTRODUCTION**

#### **1.1 Background**

Most energy supply worldwide are derived from non-renewable energy such as petroleum, oil, coal and natural gases. Due to the rapid depletion of non-renewable energy, scientist and engineers are constantly trying to develop renewable energy in order to meet the global energy demand and also to minimise the environmental impact.

Renewable energy is defined as energy that comes from resources which are made up by human timescale such as sunlight, wind, rain, waves and also geothermal heat. The renewable energy replaces the fossil fuel in four major areas, namely electricity generation, hot water heating, motor fuels and rural energy (stand-alone power systems). The types of renewable energy available in Malaysia include hydropower, wind energy, solar energy, geothermal energy and also bio-energy. The main renewable energy used in Malaysia is hydropower, due to plenty of ocean available in Malaysia. Solar energy ranked as the second main renewable energy as Malaysia enjoys sunny weather. A photovoltaic system is required to generate solar energy in the form of electrical energy.

The solar cells used in the solar panels are always connected by copper (Cu) ribbons held together by interconnection materials. The interconnection materials are usually solders and sometimes electrical conductive adhesives. The Sn-36Pb-2Ag solder is the most popular interconnection material in the world due to its low processing temperature, relatively cheap price and is usually coated on the Cu ribbon

for the ease of processing. The main disadvantages of lead (Pb)-containing solders are its environmental and health hazards. Arise from that, several types of Pb free solder were introduced to the market, among which the Sn-Ag-Cu solder is most popular to date. The main benefits of Sn-Ag-Cu solder is its relatively low melting temperature, superior mechanical properties and good solderability when compared to Pb based solder. In this project, the SAC is used as interconnection material in the bi-facial solar cells.

The photovoltaic module is made up of monocrystalline silicon solar cells (bi-facial), Pb coated Cu ribbon and Pb-free solder paste containing flux. Pt particles were added to the SAC solder paste as it is expected to increase conductivity of the solder paste. Addition of Pt is also expected to suppress excessive growth of the IMC layer as well as Kirkendall voids. According to Matthiesen's rule, presence of impurities and defects will impair electrical conductivity. The addition of Pt into the SAC solder, a lower resistivity and thus higher energy yield is expected.

## 1.2 Aims and Objectives

The aim of this research is to study the degradation of the bi-facial solar cells under the sun.

Problem Statement: How the platinum reinforcement in solder improve the performance of solar panel?

The objectives of this research are:

- 1) To fabricate an effective bi-facial solar cell with platinum reinforced solder of Sn-3.0Ag-0.5Cu-0.40Pt (SAC-0.40Pt).
- 2) To study the microstructures of SAC and SAC-0.40Pt solder on bi-facial solar panel after exposure to sunlight.
- 3) To study the microstructures of SAC and SAC-0.40Pt solder on bi-facial solar panel after heat treatment at 80°C.

- 4) To measure the resistivity for the solar cell of SAC and SAC-0.40Pt solder on bi-facial solar panel after heat treatment at 80°C.

## **CHAPTER 2**

### **LITERATURE REVIEW**

#### **2.1 Solar Cells**

##### **2.1.1 Types of Solar Cells**

The most popular and efficient solar cells are crystalline silicon solar cells and thin-film solar cells. Crystalline silicon solar cells have percentages of efficiencies in the range of 15% to 25%. The crystalline silicon form the basis of the monocrystalline and polycrystalline silicon solar cells. Due to their relatively different manufacturing process, these two types of crystalline silicon solar cells yield different silicon crystal growth. It relies on the cell cooling speed after carbothermic reduction. The size of the silicon crystals are controlled by using the speed of cooling after the 1700°C heating. The resulting crystals size were found to be larger with reducing cooling speed. The monocrystalline are made up of larger single crystal size. Besides that, monocrystalline solar cells are made out of silicon ingots in cylindrical shapes. In order to optimize the performance and lower costs of a single monocrystalline solar cell, the four sides of the cylindrical ingots are cut out into silicon wafers. On the other hand, as the result of fast cooling, polycrystalline solar cells are made up from many tiny silicon crystals (Trowbridge, 2013). Unlike monocrystalline solar cells, polycrystalline solar cells do not require the Czochralski process (Us and Maehlum, 2012). The Czochralski process is a method of crystal growth used to obtain single crystals.

Both of the polycrystalline and monocrystalline have their advantages as well as disadvantages. Monocrystalline solar cells have the highest efficiency rates since

they are made out of the highest-grade silicon (15-20%). These cells are more efficient in warm weather and efficiency decreases with ambient temperature. Besides that, under standard operating condition, monocrystalline solar cells have been proven to be more efficient as they require least space. Also, the lifespan of the monocrystalline solar cells is the longest. This can be observed whereby most solar cells manufacturers have a 25-year warranty period on their monocrystalline solar cells. However, monocrystalline solar cells are less affordable due to their most expensive pricing among all solar cells.

The production cost of polycrystalline cells is less as the process to produce polycrystalline silicon is simpler. Unlike monocrystalline solar cells, polycrystalline solar cells have greater efficiency with increasing ambient temperature. Despite that, the overall increased efficiency is still of 3-4% less than that of the monocrystalline solar cells. Thus, more space will be required to produce the same amount of power compared to monocrystalline solar cells.

Thin-film solar cells are produced by a way of depositing one or several layers of electrical conductive or photovoltaic material onto a substrate by a method called chemical vapor deposition (CVD) process. The different types of thin-film solar cell can be categorized by which photovoltaic material is deposited onto the substrate:

- Amorphous silicon (a-Si)
- Cadmium telluride (CdTe)
- Copper indium gallium selenide (CIS/CIGS)
- Organic photovoltaic cells (OPC)

The substrate deposited with amorphous silicon (a-Si) are also known as the amorphous silicon cells and are able to absorb light easier compare to crystalline solar cells as they do not have crystalline structure. Thus, the cell fabricated can be thinner. However, the overall conversion efficiency is lowest among other mentioned solar cells (Us and Maehlum, 2012).

### 2.1.2 Advantages and Disadvantages of Solar Energy

The photovoltaic system using solar panels provide clean and green energy unlike other energy sources. During electricity generation for photovoltaic panels, there is no greenhouse gas emissions harmful to the environment, thus the solar PV is more environmentally friendly compare to other renewable energy. Besides that, the solar energy is a natural energy produced by the sun and it is free and abundant. The photovoltaic panels are also totally silent and is able to prevent noise pollution.

Among disadvantages of the solar energy, is its inability to outperform in terms of energy production when compared to other renewable sources. This is because the conversion of light energy from the sun to generate electricity through the photovoltaic effect is not perfect due to frequency of incident light on the solar modules. The effectiveness of the solar cell is related to the conversion rate of the sunlight, and the conversion rate for the mono-facial solar cell are in the range of 10% to 20%. Each side of the bi-facial solar cell have the same conversion rate as mono-facial solar cell. The current best achieved sunlight conversion rate for solar module is about 21.5% in a new commercial product by SunPower cooperation (SunPower e20 Module, 2013).

The efficiency of the photovoltaic system relies on solar intensity level, types of solar cell, materials used in manufacture of solar cells, solar modules, solar panel, and also arrays pattern. The wiring connection method between the individual solar cells will also affect the performance of the PV system.

The effectiveness of the solar cell is calculated by applying the following equations which is power output of the solar cell over power input from the sun (Emery & Osterwald, 1986). The incident power from the sun mainly depend on the climate, location and also season whereby the system is located.

$$\% \text{ Efficiency} = \left( \frac{\text{Maximum Power Generated, } P_m}{\text{Incident power from Sun, } P_{in}} \right) \times 100 \quad (2.1)$$

where:

The maximum power generated by the solar cell is in units of W/m<sup>2</sup>.

$$P_m = \frac{\text{Voltage}, V \times \text{Current}, I}{\text{Area}, A} \quad (2.2)$$

## 2.2 Bi-facial Solar Cells

### 2.2.1 Fundamentals of Bi-facial Solar Cells

The bi-facial solar cells is a two-sided device capable of converting solar radiance from sun into electricity at each surface.

The first two p-n junction solar cell with p<sup>+</sup>-n-p<sup>+</sup> structure was firstly proposed by H. Mori. It is to generate a p-n junction at every side of the silicon wafer surfaces to form bi-facial double junction solar cells. The rear side p-n junction was used to intensify the solar irradiance collection efficiency for long-wavelength photons (Cuevas, 2005).

Other than p<sup>+</sup>-n-p<sup>+</sup> structure, many researches also work on the solar cells with n<sup>+</sup>-p-n<sup>+</sup> (Ohtsuka, et al., 2000). Researches of Ohtsuka, et al. (2000) at Polytechnical University of Madrid uses n<sup>+</sup>-p-n<sup>+</sup> structure with a 4cm<sup>2</sup> area and low quality material to fabricated a solar cells device with an efficiency of 12.7%.

The bi-facial back surface field (BSF) solar cells consisted of single p-n junction and a high-low junction. The ideal of creating this kind of solar cells is proposed by the passivation effect of the floating n<sup>+</sup> diffusion into n<sup>+</sup>-p-n<sup>+</sup> structure. These cells have a homopolar junction on the other surface of a heteropolar p-n junction. The heavily doped region was doped with chemical element through diffusion method, such as p<sup>+</sup> type layer is doped with boron while n<sup>+</sup> type layer is doped with phosphorus. This region reduces the crossing over at the rear surface and thus enhances open-circuit voltage. In year 1970, the first BSF cell was actually a bi-facial cell which produced at Russia and patented by Bordin et al.

### 2.3 Degradation of Solar Modules

The sustainability of the solar modules is mainly determined by the stability and resistance to corrosion of the materials used to build the solar modules. The most common degradation and failure modes on solar module are caused by water ingress and temperature cycling. All external factors of degradation will cause the solar module efficiency to decline over time. The degradation can be caused by increases in surface resistance caused by decreased adherence of contacts or corrosion which is usually caused by water vapour, decreases in shunt resistance due to metal migration through the p-n junction and antireflection coating deterioration.

Besides that, potential induced degradation (PID) often occurs in the solar modules once operation starts. PID is an undesirable occurrence in solar modules which occurs when the module's voltage potential and leakage current drive ion mobility within the module between the semiconductor material and other components in the module. The speed of ion mobility occurring within the module increases with humidity, temperature and also voltage potential.

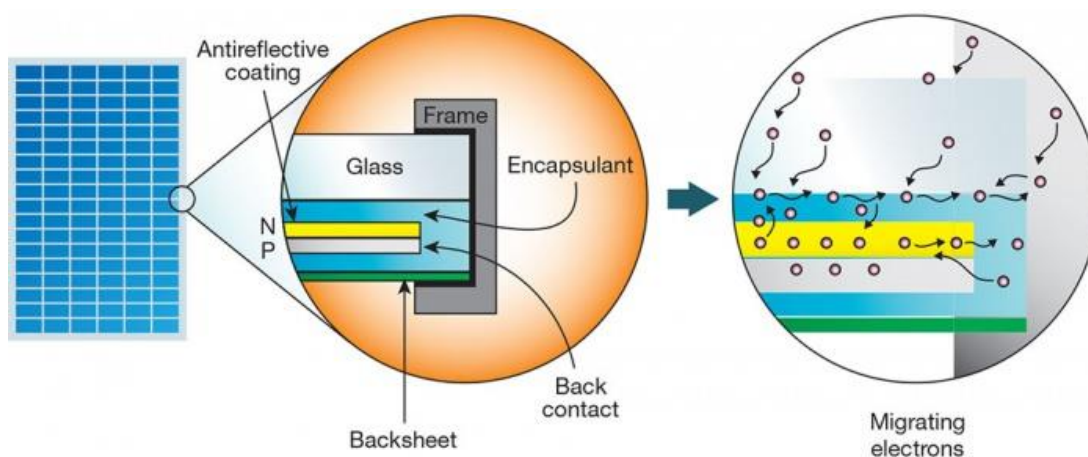


**Figure 2.1: Leakage Current and Voltage Potential (negative potential shown) Cause Negative (-) Ions to Migrate Away from the Semiconductor, as Positive (+) Ions Migrate Toward the Semiconductor from the Glass and Package, and the Module's External Environment (Advanced Energy, 2013)**

Pingel, S., et al. (2009) reported that the base doping of element was varied by almost two orders of magnitude. The Figure 2.2 shown that the increase on base resistivity leads to PID because a lower base doping would lead to a wider depletion region at the junction.

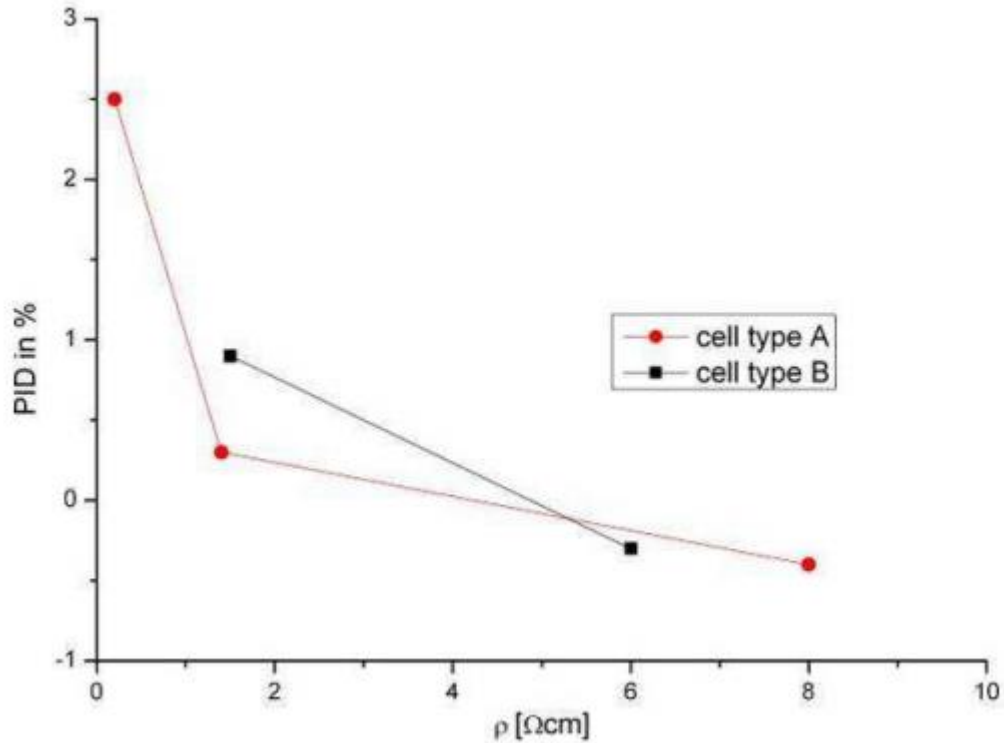


**Figure 2.2: Base Resistivity Dependence of PID (Pingel, S., 2009)**

Extended defects, such as grain boundaries and dislocations, might carry electrical charge and then act as efficient recombination centres. The electrical activity of these defect centres is largely influenced by their interaction with impurity atoms and usually increases with increasing impurity concentration (Thompson et. al., 1999).

Metal resistance also influences the performance of solar modules. According to Matthiesen's rule, the total resistivity of a metal specimen are contributed by thermal vibrations, impurities, and plastic deformation where it could be represented in a mathematical form of

$$\rho_{total} = \rho_t + \rho_i + \rho_d \quad (2.3)$$

where  $\rho_t$ ,  $\rho_i$ ,  $\rho_d$  represent individual thermal, impurity and deformation resistivity contribution respectively (William and David, 2010).

## 2.4 Lead-Free Solders

The tin-lead (Sn-Pb) solders are widely used as the interconnecting material in electronic devices due to its reliable and robust solder joint. Besides that, Sn-Pb solder also have low melting point property and good wetting behaviour which lead to good solder joint with the substrate plating on the ribbon. Other than that, Sn-Pb solders also creates metallization layer for soldering on substrate plating and create strong intermetallic bond between the solders and substrate plating. Due to the environmental and health issues on the society, the Sn-Pb solder is being replaced by a variety of new Pb free solders.

A common problem due to application of the Pb free solder is the increase of thickness of the IMC layer which will reduce the electrical conductivity. Kirkendall voids form from the  $\text{Cu}_3\text{Sn}$  layer of the IMC, compromising the solder joint reliability (Y.W. Wang & Lin, 2008). This causes the strength of the solder joint and drop test performance to be significantly reduced. Masazumi Amagai (2008) found that Kirkendall voids under the IMC layer can reduced by adding Nickel (Ni) and also Indium (In) to the solder. Besides that, the combination of Cu and Phosphorus (P) will significantly reduce the IMC layer thickness. Amagai also found that by adding Cobalt (Co), Ni, or Pt which located at the left of Cu in periodic table into tin-silver (Sn-Ag) based solder alloys, the IMC thickness and grain size of the solder did not increases significantly after the solder reflow process and thermal aging.

Kim & Kim (2004), conducted a study whereby Pt was added into the Sn-Ag based solder alloys because it has a dismissing rate similar to Ni and has a great oxidation resistance when compared to other metal although it is more expensive.

## 2.5 Intermetallic Reaction and Growth of Solder Paste with Pt

During the reflow process, the IMC structure will be formed between the solder particles and metal layer by interdiffusion kinetics. The interdiffusion kinetics is shown in Equation 2.4

$$d = d_o + \sqrt{Dt} \quad (2.4)$$

where  $d_0$  is the initial thickness,  $D$  is diffusivity, and  $t$  is time. The diffusion component can be described by an Arrhenius equation as such

$$D = D_0 e^{\left(-\frac{Q}{kT}\right)} \quad (2.5)$$

where  $D_0$  is a constant independent of temperature,  $Q$  is activation energy,  $k$  is the Boltzmann constant, and  $T$  is absolute temperature. Holding the peak temperature during reflow for longer durations increases the initial IMC layer thickness and changes the morphology (Crandall, 2011).

The interfacial reaction of Sn-3.8Ag-0.7Cu solder paste and Pt was studied after reflow process. This is due to the detection of IMC at the solder paste or Pt interface containing  $\text{Cu}_6\text{Sn}_5$ ,  $\text{PtSn}_4$ , and  $\text{Ag}_3\text{Sn}$  inside. The  $\text{Ag}_3\text{Sn}$  phase was formed when the compound were dispersed throughout the solder alloy. As reflow time increases, these phases will increase in size. Besides that, the interfacial IMC thickness also increases with the reflow time.

$\text{Cu}_6\text{Sn}_5$  was found to be randomly distributed inside the solder alloy after the reflow process or thermal aging. This type of intermetallic phase consists of long and larger compounds which form by the mixing of Cu and Sn in the solder paste. This phase can only be formed in the solder pastes containing of Cu element. This compound was not found near the Pt interface before reflow process. However as reflow process prolongs, it tends to move away from the Sn-Ag-Cu interface. Lastly, contact angle between  $\text{PtSn}_4$  and  $\text{Cu}_6\text{Sn}_5$  was increased when the reflow time increased.

The  $\text{PtSn}_4$  IMC grows fast in the Sn-Ag-Cu solder. The  $\text{PtSn}_4$  IMC structure forms even more rapidly when there is fewer Cu content in solder when compare to Sn element. This is because solder has low melting point and there are more Sn content in facilitating the  $\text{PtSn}_4$  phase formation. Under the identical reflow condition,  $\text{PtSn}_4$  IMC formed at the interface between solder which contains a small amount of Cu and Ni substrate has higher growth rate compared to the compound formed at the Pt interface. Therefore, slow growth rate of  $\text{PtSn}_4$  is one of the advantages of Pt as a metallization layer (Kim & Kim, 2004).

In this research,  $\text{Cu}_3\text{Pt}$  phase is formed through the interdiffusion between the two material of Pt and Cu in thin films. It is difficult for diffusion of Cu into Pt, therefore Pt-Sn intermetallic formation would be more favored. Besides that, a parabolic relationship between the thickness of the Pt-Sn intermetallic and reaction time indicates the intermetallic formation in the solder/platinum interface is diffusion controlled (Kim & Kim, 2004). Lastly, in the research of S.J. Wang and C.Y. Liu, dissolution of the Pt will cause the Cu to be less soluble on the molten solder (Wang & Liu, 2007).

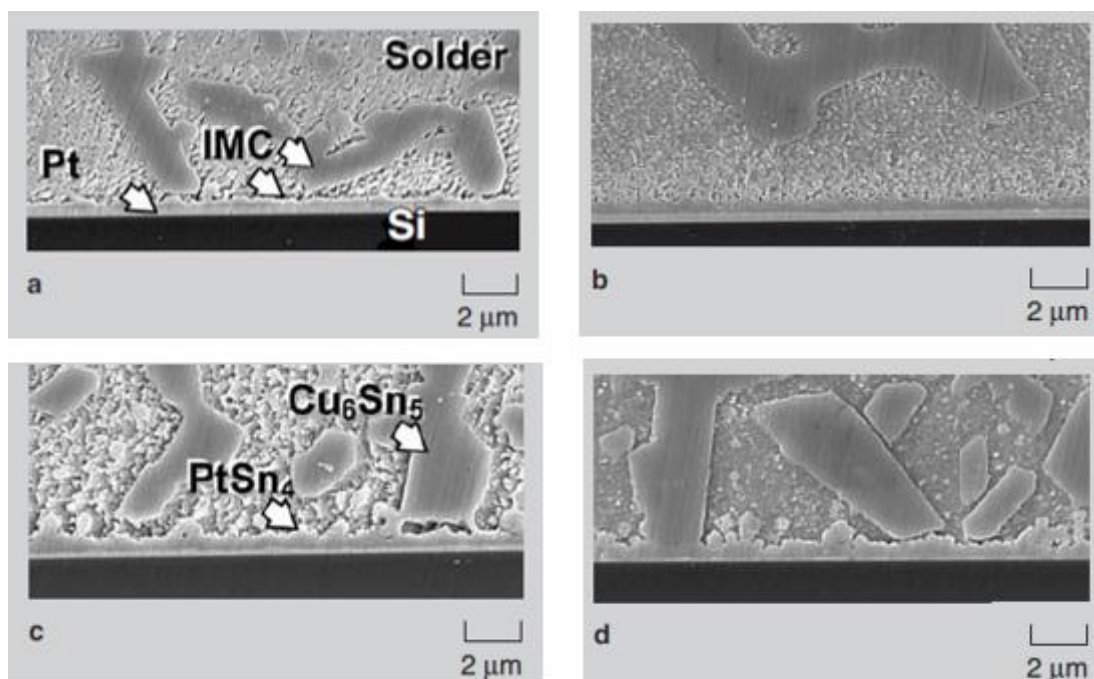


**Figure 2.3: The Intermetallic Microstructure of Sn-3.8Ag-0.7Cu Solder after Reflow at (a) 30 s, (b) 90 s, (c) 360 s, and (d) 600 s (Kim & Kim, 2004)**

## 2.6 Addition of Different Elements to Solder Paste

The addition of rare earth elements into solder paste can significantly enhance the properties of solder paste such as wettability and spreading properties, melting temperature, mechanical properties of soldered joints, and the reaction interface of solder paste.

Lili Gao & Songbai Xue (2010) reported that the wetting and spreading properties can be improved by adding cerium (Ce), Bi, gallium (Ga), In and Ni as it increases the wettability and spread rate of the solder paste. The wetting force and wetting angle is also important in order to produce a good metallurgical bonding. The wetting force of conventional Sn-Ag-Cu solder pastes will increase when the appropriate amount of rare earth elements are added. When the wetting force increased, the wettability will also increase. Thus, the solder paste easily wets and bonds with the substrate it is applied onto. The wetting angle can also be reduced by rare earth elements.

The addition of rare earth elements on Sn-Ag-Cu solder paste does not have a significant effect on the melting temperature on the solder alloys. S. Lu & Y. Chen (2008) reported that addition of magnesium (Mg) in the Sn-Ag-Cu solder paste will reduce the melting temperature of the solder. Besides that, it is also found that the more the Mg is added in the solder paste, the more the melting temperature decreased.

The mechanical properties of the solder paste will also be reduced when the Co and iron (Fe) rare earth elements are added. The tensile strength between the solder paste and substrate will be increased when the Co and Fe are added on the solder paste. The high tensile strength ensures the high structural reliability of the solder joints. Whereas, from the research of L.W. Lin & J.M. Song (2009), the addition of manganese (Mn) and titanium (Ti) will lower down the strength of solder paste but improved the ductility of the solder paste. Lastly, the addition of zinc (Zn) in solder paste has an effect of reducing the undercooling efficiency and restricts the growth of Ag<sub>3</sub>Sn IMC layers at the interface of solder-silver (Ag) busbar.

Lastly, the addition of cerium (Ce) can refine the microstructure and reduce the amount of  $\text{Ag}_3\text{Sn}$  phase besides control of the IMC layer thickness.

## **2.7 Reflow Soldering**

In preparing the solar cells, a solder paste is used to attach the Cu ribbon used as conduct of the bi-facial solar cells and the entire assembly is subjected to controlled heat. This is known as reflow soldering. Controlled heating is required to melt the solder paste and to form the metallurgical bonding. The heating can be accomplished by pass of assembly through reflow oven, or using infrared lamp or hot air pencil to individually soldering the joints.

The busbar of the bi-facial solar cells is coated with solder paste by screen printing. The screen printing is a manual method to apply the solder to the busbar of solar cells by using squeegee and stencil. The Cu ribbon will then be placed according to the area of busbar with solder. After that, the Rosin Mildly Activated (RMA) flux is applied between the solder and the Cu ribbon. The whole assembly is then to be heated in the oven in accordance to a pre-determined reflow profile.

### **2.7.1 Reflow Specification**

The reflow specification is crucial to obtain a good quality and high reliability of solar cells. Thus, the reflow profile of solder paste is used for soldering process. The high quality of soldering and lower rate of defects are required to be supplemented by an optimal reflow soldering profile. It can be described using reflow profile provided by RedRing Solder. Normally, the profile consists four different zones or phases, which are the preheat zone, soak zone, reflow zone and the cooling zone. Thus, every zone will have their own heating rate, duration and also maximum temperatures which are setting according to the solder paste properties.

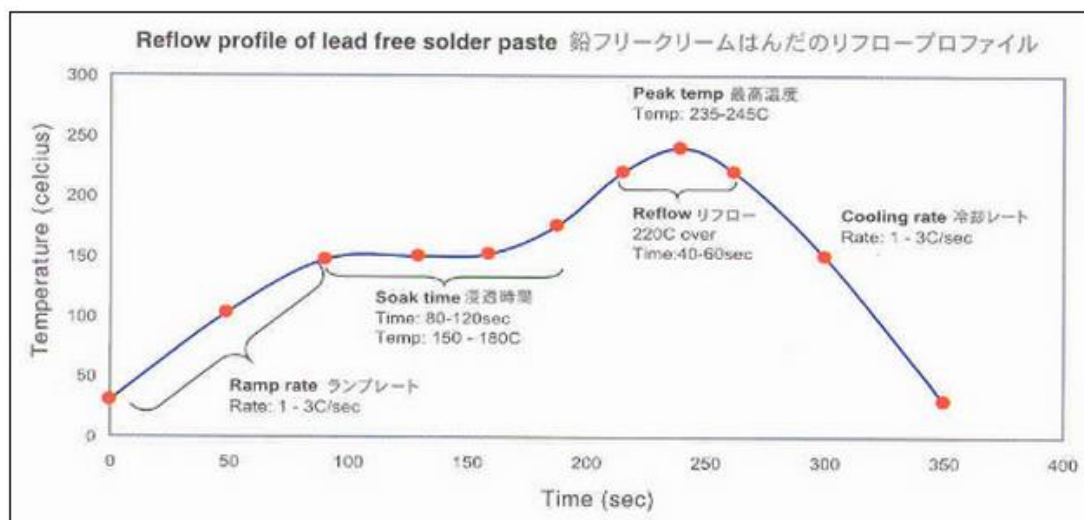


**Figure 2.4: Reflow Profile for Lead Free Solder Paste (RedRing Solder, 2013)**

In the preheat zone, heat rate must undergo changes from 1°C per second to 3°C per second. Meanwhile, peak temperature should achieve in the range of 100-150°C. The changing heating rate must be low to avoid the splatter of solder paste which will causes the formation of solder balls. Lastly, a gradual and slow temperature ramp must be supervised and controlled to avoid of exposing solar cell to thermal shock.

In soak zone, which is known as the flux activation zone, changes in temperature must be slowed down to diminish the temperature gradients. The ramp rate is nearly even with the temperature increasing near to the melting point of solder as shown in figure below. The fluxing activation was carry out in the solder paste at this zone. If the heating temperature is too much excess of the required temperature, there will be inadequate fluxing in solder paste and the solder splatter due to unnecessary oxidation on the solder paste. This zone usually carried out in the temperature range between 150 °C to 180 °C for 80 to 120 seconds.

Next, in the reflow zone, the temperature of heating is adjusted beyond the melting point of the solder for about forty to sixty seconds is to ensure sufficient flux action in the solder and to obtain good wetting properties. Typically solder paste has the melting point from 215 °C to 225 °C. However, peak temperature must monitored in order to avoid excessive heat which will cause damages on the solar cells. Besides

that, high temperature will promote oxide growth which reduces the solder wetting properties.

Lastly, the assembly of the Cu ribbon with solar cell will be left to cool, this part is known as the cooling zone. In cooling zone, the cooling rate was brought to 1 to 3 °C per second. Smaller grain sizes of solder will induce rapid cooling hence increases solder joint's fatigue resistance. However, rapid cooling rate will cause mismatch between residual stresses and thermal coefficient of expansion. This would also affect the mechanical properties of solder joints since the cooling rate are directly related to the growth of microstructure. Therefore, it is important to maintain and monitor the cooling rate for the reflow soldering process to produce high reliability solar cells (Anadigics, 2001).

## CHAPTER 3

### METHODOLOGY

#### 3.1 Materials and Methods

##### 3.1.1 EarthON Bi-facial Solar Cells

EarthON monocrystalline bi-facial solar cells manufactured by PhotoVoltaic Global Solutions Inc. are used in this study. The solar cell metallization is made of Ag on both sides. Solar cell metallization forms several thin fingers and three white thick busbars which is perpendicular to thin fingers on both sides of the solar cells. The three thicker busbars are used for soldering with Cu ribbon to conduct electricity. The front side of solar cell consists of p-type layer, while the rear side has n-type wafer and n<sup>+</sup> layer.

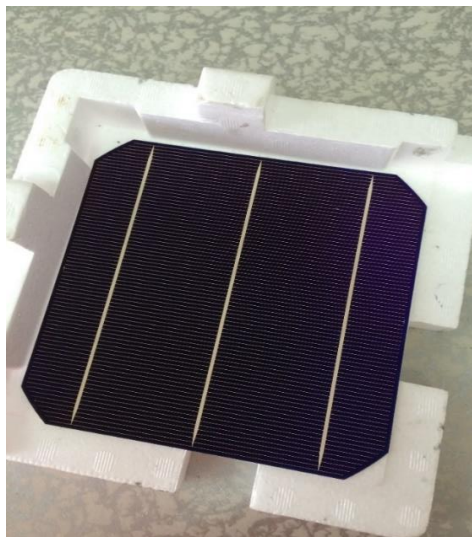


**Figure 3.1: EarthON Bi-facial Solar Cell**

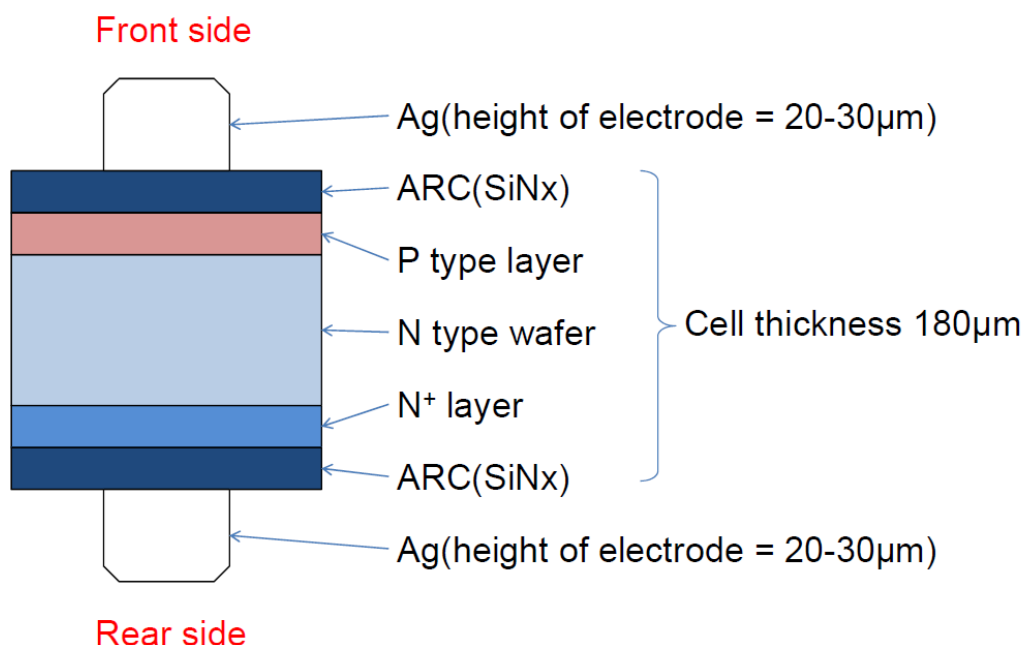


**Figure 3.2: Cross Section of p-n-n<sup>+</sup> Bi-facial Solar Cell (PVG Solutions Inc, 2011)**

Usually, the monocrystalline solar cell has dark colours, such as dark blue. As a result of manufacturing method and normal trait of the monocrystalline silicon, the cells do not have pointy corners (Martin, 2012). Besides that, the bi-facial solar cell has identical front and rear faces, but can be distinguished through observing middle finger on each side of the solar cell. The middle finger of rear side has a vertical line that forms “T” shape. Whereas, the middle finger on the front side has a vertical line that forms “+” sign with the finger (PVG Solution Inc, 2011).

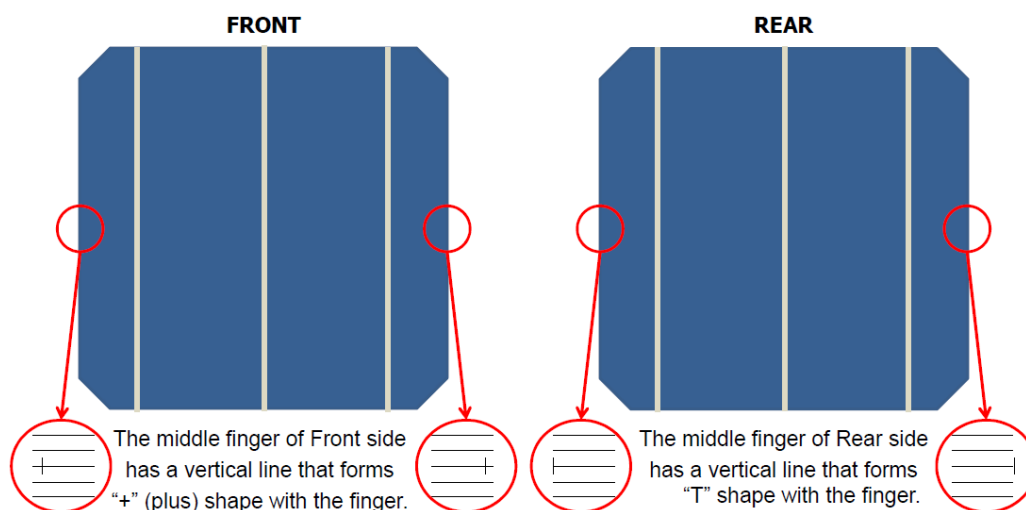


**Figure 3.3: EarthON Bi-facial Solar Cell**

Dimensions of the EarthON Bi-facial Solar Cell are shown as figure below,

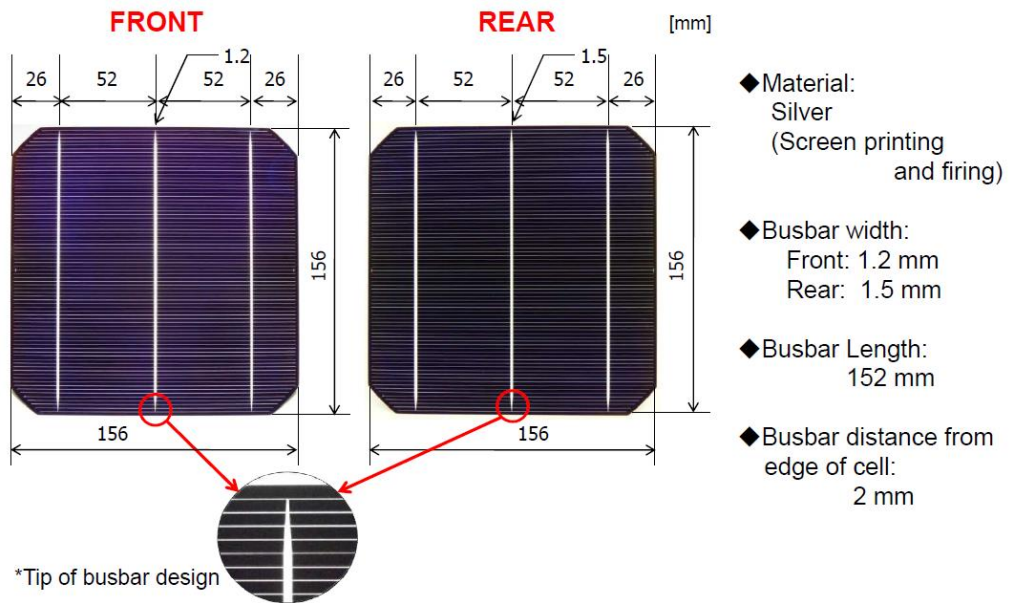


**Figure 3.4: Dimension of EarthON Bi-facial Solar Cell**

Table 3.1 shows the recommended soldering condition provided by PhotoVoltaic Global Solutions Inc. In order to maximize the conversion of light to electrical energy, it is important to match the band gap energy with the spectrum of light. Figure 3.5 shows the spectral response of EarthON bi-facial solar cells on both sides to wavelength of light.

**Table 3.1: Recommended Soldering Condition for EarthON Bi-facial Solar Cell**

Item	Condition
Tabbing ribbon	Solder plated copper strips
Core Cu thickness	0.15 - 0.20 [mm]
Core Cu width	1.2 - 1.5 [mm]
Solder plated thickness	10-30 [ $\mu\text{m}$ ] per side
Solder content	Sn 60 % / Ag above 2 % / Pb
Flux RMA type	Low solid content type.
Preheating	100-140 [ $^{\circ}\text{C}$ ] *depends on equipment and flux
Soldering temperature	190-290 [ $^{\circ}\text{C}$ ] *depends on equipment and flux
Soldering process	Both front-side and rear-side soldering simultaneously

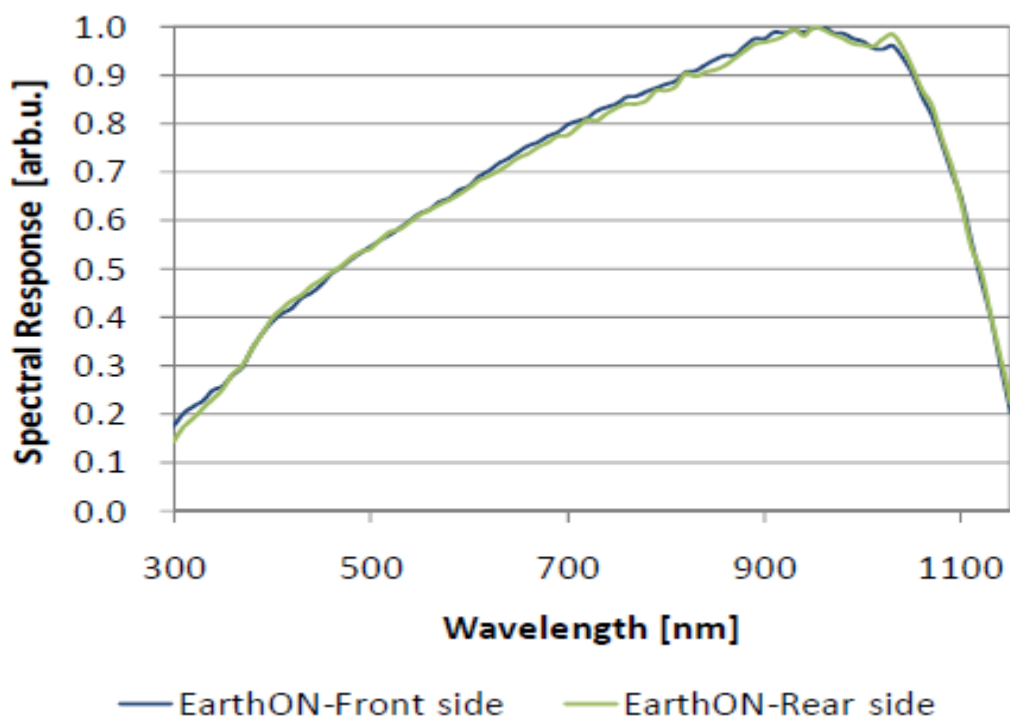


**Figure 3.5: Spectral Response Data**

### 3.1.2 Lead Coated Ribbon

The soft Luvata Sunwire Pb coated Cu ribbon was used to be soldered onto the busbars of the bi-facial solar cells. It has quicker throughput and lower yield strength. Lower yield strength will prevent tension to be created in the solar cells during reflow (Luvata, 2010).



**Figure 3.6: Luvata Sunwire of Lead Coated Copper Ribbon**

### 3.1.3 Solder

The solder used in this study is SAC. 0.40 wt.% of Pt particles were added to the solder paste. The solder used has minimal residual flux production and is translucent, therefore does not hinder the surface of the solar cell from absorbing the sun rays. The solder paste has a melting range between 217-225°C (RedRing Solder, 2013). The solder paste is stored in the refrigerator which have a temperature range from 0-10 °C.



**Figure 3.7: RedRing Solder Paste**

### 3.1.4 Rosin Mildly Activated (RMA) Flux

Rosin Mildly Activated (RMA) flux is used in the production of the bi-facial solar cells. It has high thermal stability, excellent fluxing ability with instant wetting and low surface tension. The RMA flux also leaves behind little flux residue, is non-corrosive and non-tacky after soldering process (RedRing Solder, 2013).

### 3.1.5 Weifo Microprocessor Controlled Programmable Oven

Reflow soldering was carried out in the Weifo OV200S Oven. Temperature calibration was done during the first 20 minutes using a thermometer until the temperature stabilises. This is to ensure accuracy of the oven temperature.

## 3.2 Inclusion of Platinum into Solder Paste

0.40 wt.% of Pt particles were dispersed into the SAC solder and stirred until homogeneous. Equation 3.1 and Equation 3.2 shows calculation of amount of Pt particles to be added to the solder paste.

$$\frac{M_{Pt}}{M_{Pt} + M_{SnAgCu}} = wt \cdot \% \quad (3.1)$$

$$M_{Pt} = \frac{(wt\%)(M_{SnAgCu})}{1 - wt\%} \quad (3.2)$$

where,  $M_{Pt}$  is mass of Pt particles,  $M_{SnAgCu}$  is mass of SAC solder paste and wt.% is weight percentage of Pt in the solder paste.

## 3.3 Pre-Soldering Preparation

Paper stencil as shown in Figure 3.8 is used for reflow soldering. The Pt particles will be stirred into the SAC solder paste and applied onto busbar with the help of paper stencil. The Cu ribbons were cut into lengths of 17cm each from the roll of Luvata Sunwire Cu ribbon and manually straightened and flattened to ensure precise placing on the busbar. RMA flux was brushed onto the busbar before application of solder paste to ensure optimum solderability. Cu ribbons was then applied onto the solder paste located at busbar. These steps were repeated for the rear side of the solar cell.

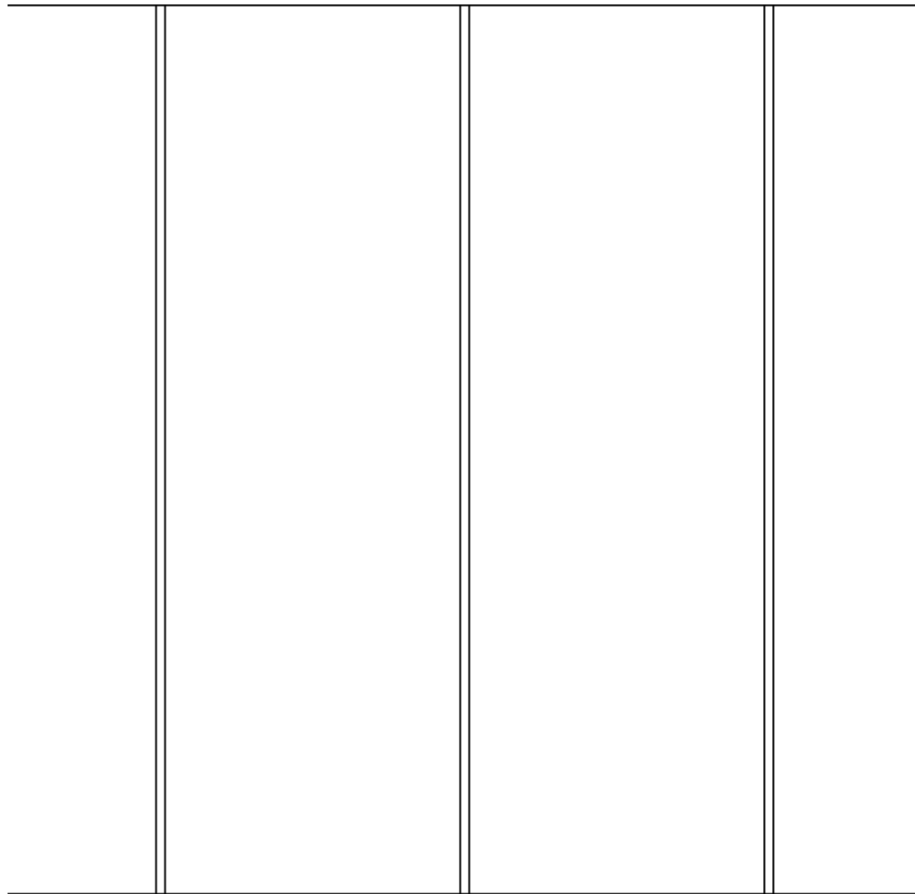


**Figure 3.8: Sample of Custom Made Paper Stencil**

The dimension for the custom made paper stencil used in the resistivity test for the bi-facial solar cells is same as the custom made paper stencil for reflow soldering with the transfer length dimensions added in. The transfer length of the custom made paper stencil for resistivity test consists of thirteen squares with the dimension of  $1.5\text{mm} \times 1.5\text{mm}$ . The distance between each square is different. The Cu ribbons were cut into squares of  $1.5\text{mm} \times 1.5\text{mm}$  each from the roll of Luvata Sunwire Cu ribbon followed by straightening and flattening. After that, the flat Cu squares were allowed to adhere on the busbar with the solder paste on it. Flux is added to improve solderability.

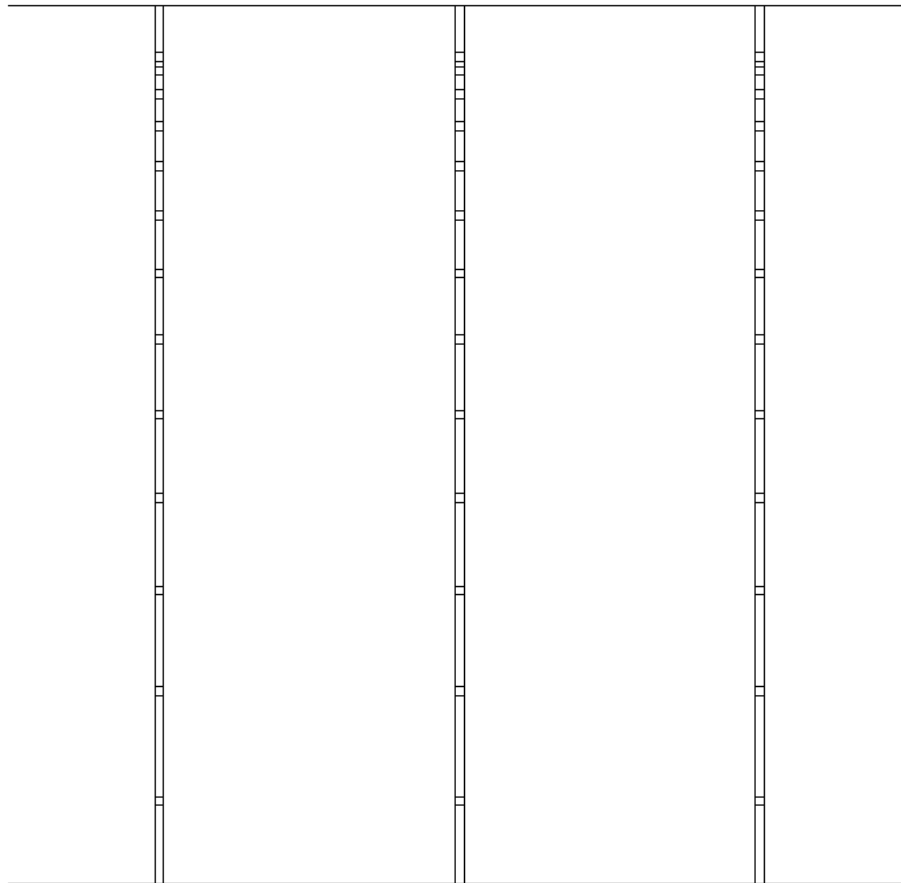


**Figure 3.9: Sample of Custom Made Paper Stencil for Resistivity Test**

### **3.4 Bi-facial Solar Cell Soldering**

After the Cu ribbons were held in place by the solder paste, the solar cell is placed on a clean ceramic tile and reflowed in a microprocessor controlled programmable oven.

The reflow temperature profile for reflow soldering of bi-facial solar cell process is shown in Figure 3.10. Initially, the temperature was set at 225°C for the first one hour and the next temperature set point was at 25 °C from one hour to three hours and twenty minutes. This is indicated by the red line in Figure 3.10. The first temperature set point is known as the heating phase, whereas the second temperature set point is known as the cooling phase. The actual temperature inside the oven was slowly increased up to 240°C and left constant for five minutes to initiate the soldering flux reaction and solder reflow reaction respectively. After that, the oven was allowed

to be cool down to room temperature. The steady cooling was designed for reduce large thermal shrinkage which will damage the solar cells.

The solar cell then removed carefully from the ceramic tiles using hard Ag ribbon. This is because the solar cell may stick on the ceramic due to excessive solder paste or flux.

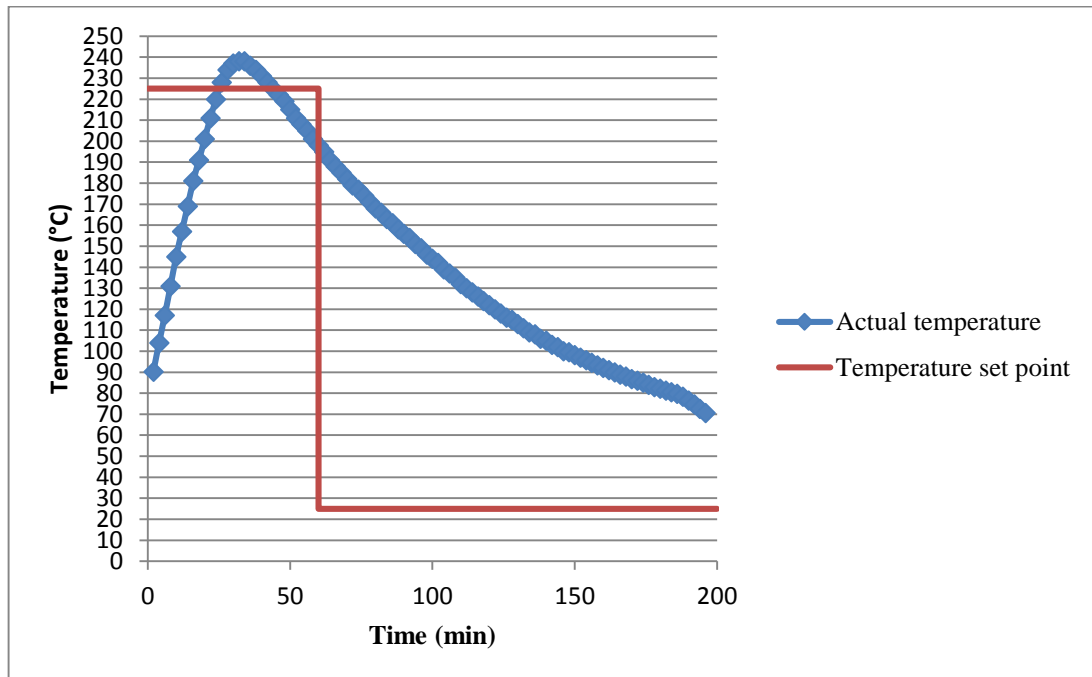


**Figure 3.10: Reflow Temperature Profile (Weifo, 2013)**

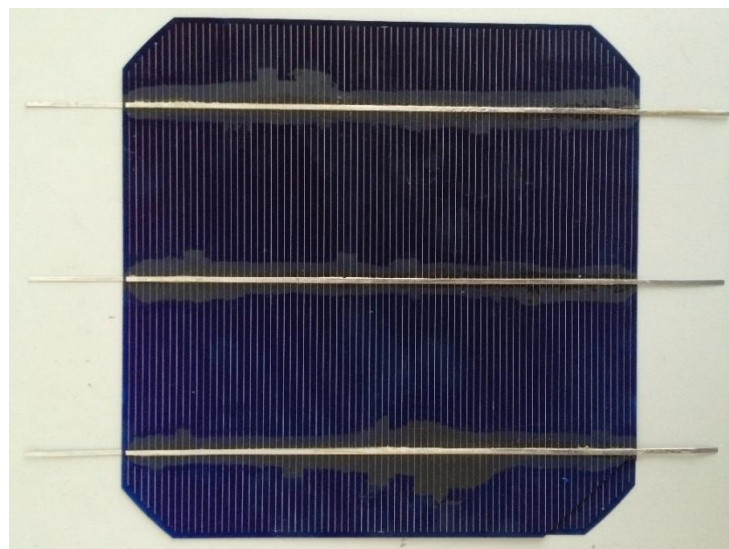


**Figure 3.11: Soldered Bi-facial Solar Cell**

### 3.5 Encapsulation Process

The purpose of the encapsulation process is to protect the cells and their interconnections from the environment. The encapsulation will prevent the solar cell metallization and the interconnecting ribbons from oxidation due to the exposure to rain and water vapour.

In this project, acrylic was chosen as encapsulation material since it has high resistance to weather changes, low UV sensitivity, and optical clarity. Acrylic also has lower weight, thus is able to reduce the overall weight of the solar panel.

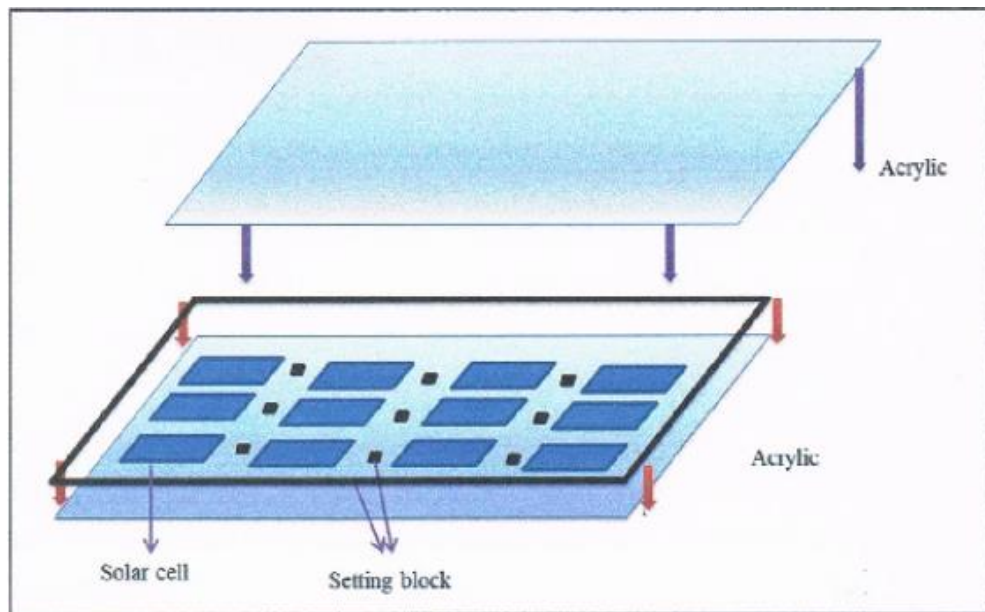


**Figure 3.12: Schematic of the Encapsulation Process**

The solar cells were encapsulated in a sandwich of acrylic with setting blocks made up of rubber located in between to create space for the solar cells to be placed and also avoid contact of the two pieces of acrylic with the solar cells. Before the encapsulation is done, silica gels must be placed in the encapsulation panel to absorb residual moisture trapped in the solar panel once the acrylic is sealed. The silica gels were prepared by heating in the furnace to remove their moisture content and wrapped in a medical dressing gauze bandage. The silica gel package is attached to the acrylic panel by using glue.

Lastly, clear silicon sealant was applied to all sides of the acrylic and block setting to seal the solar panel with the used of G-clamp. This process is to avoid any water or air entering the solar panel and causing damage to it.

### **3.6 Solar Cell Microstructure Study Preparation**

For microstructural studies, the soldered joints of the solar cell would need to be broken down into pieces in order to obtain the sandwich. The sandwich was made up with copper ribbon, bi-facial solar cell and solder paste in between. This is the initial preparation step for the solar cell microstructural study. The soldered joint sandwich structure is critical for observation of the IMC layer formation at the soldered joints of solar cell.



**Figure 3.13: Soldered Joint from the Solar Cell**

### **3.7 Specimen Preparation**

The first set of sample involves exposure of SAC and SAC-0.40Pt solar cells under the sun for a period of five weeks. The second set of samples were heat treated at 80°C for 1,3,5,12,24 and 48 hours respectively.

Both set of samples were prepared for metallographic examination. Segments of samples were cross-sectioned, mounted, grinded and polished to a mirror-like surface before etching in 98% ethanol-2% hydrochloric acid (HCl). Microstructural studies were carried out using optical and SEM. Phase identification was carried out using the EDX spectroscopy. A separate set of samples were also prepared and heat treated at 80°C for resistivity test.

#### **3.7.1 Resistivity Measurements for Solder Contact**

The solder contact resistance is measured using a high sensitivity multimeter. Samples were prepared by soldering 1.5mm×1.5mm square pieces of copper ribbons onto the bi-facial solar cell busbar containing SAC and SAC-0.40Pt solder paste with the helped of custom stencil. The contact resistance of the bi-facial solar cell is measured using the transfer length method. The contact resistance of a section of the busbar and two solder joints with distance  $d_n$  in between is measured. The Figure 3.14 shows the stencil used for soldering onto the bi-facial solar cells and the points used to measure the solder contact resistance.

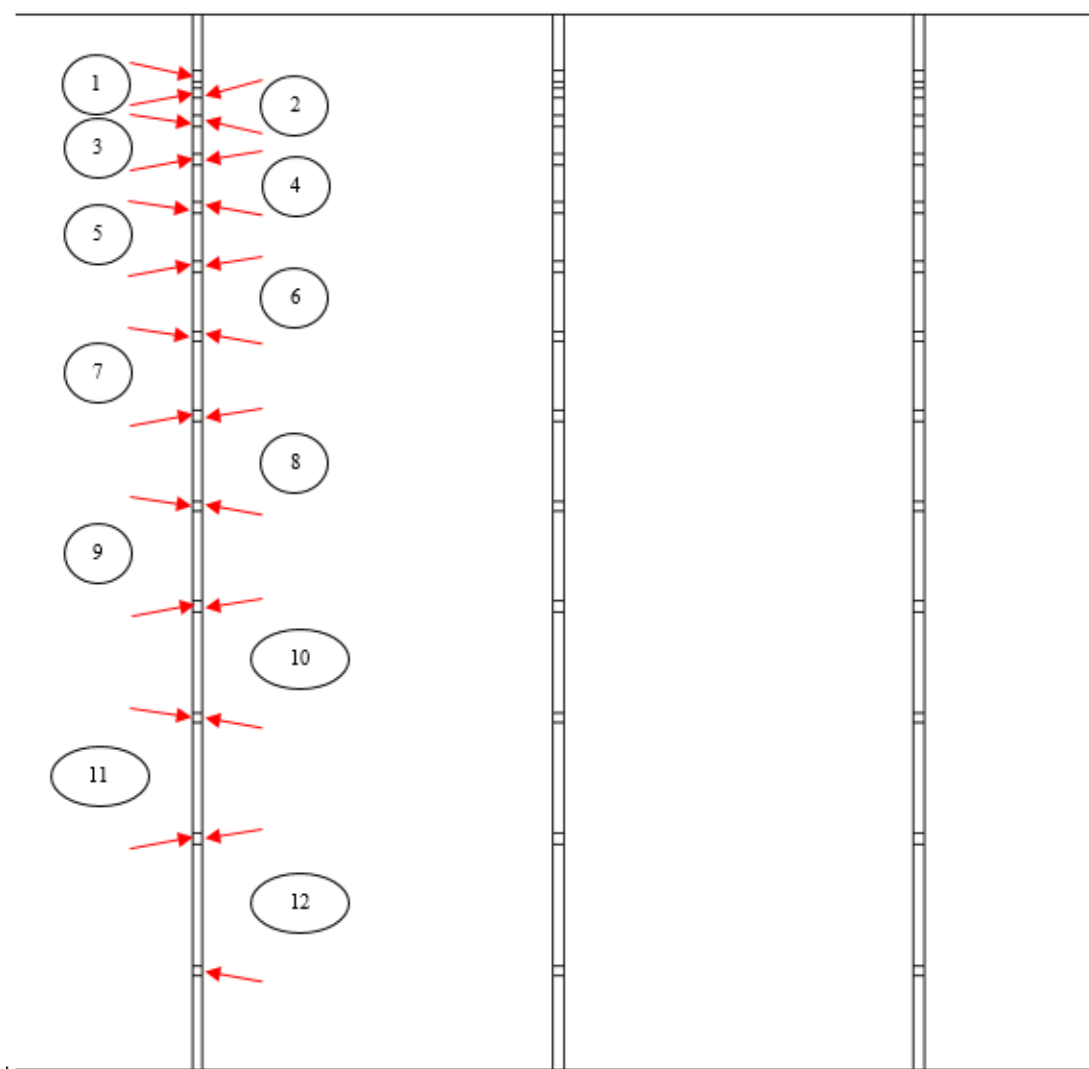


**Figure 3.14: Custom Made Paper Stencil for Resistivity Test and Points Use to Measure the Resistivity of Bi-facial Solar Cells**

The resistance of a section on the bi-facial solar cell is measured by connecting the DC power supply with constant current to the solar cell and measuring the voltage across the solar cell connection. Figure 3.15 shows schematic of the electrical circuit used to measure the resistance of a section of the busbar and two solder joints with distance  $d_n$  in between.

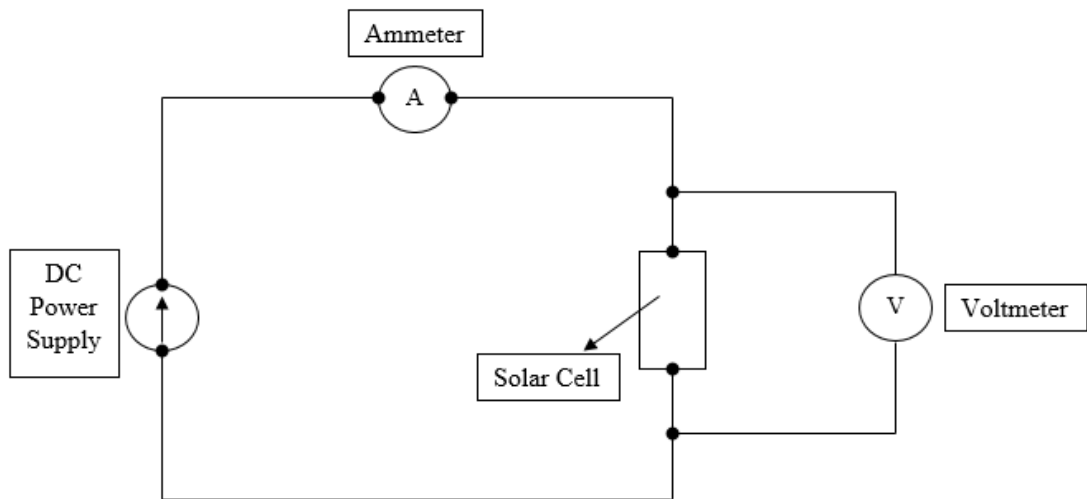


**Figure 3.15: Electrical Circuit Use to Measure Resistivity of the Bi-facial Solar Cells after Heat Treatment**

The voltage of the solar cells were measured twice for each samples for the variation in Cu ribbon surface quality when the measuring probes were placed at different contact points on the solder joints. The total contact resistance is calculated by using Ohm's law.

$$\text{Ohm's Law, } V = IR_T$$

$$\text{Rearrange: } R_T = \frac{V}{I} \quad (3.3)$$

Where:  $V$  is the voltage measure from solar cells (mV)

$I$  is the current which set at DC power supply (mA)

$R_T$  is total contact resistance ( $\Omega$ )

The solder contact resistance of one section with a pair of solder joints is measured and modelled using the calculation model shown in Figure 3.16.

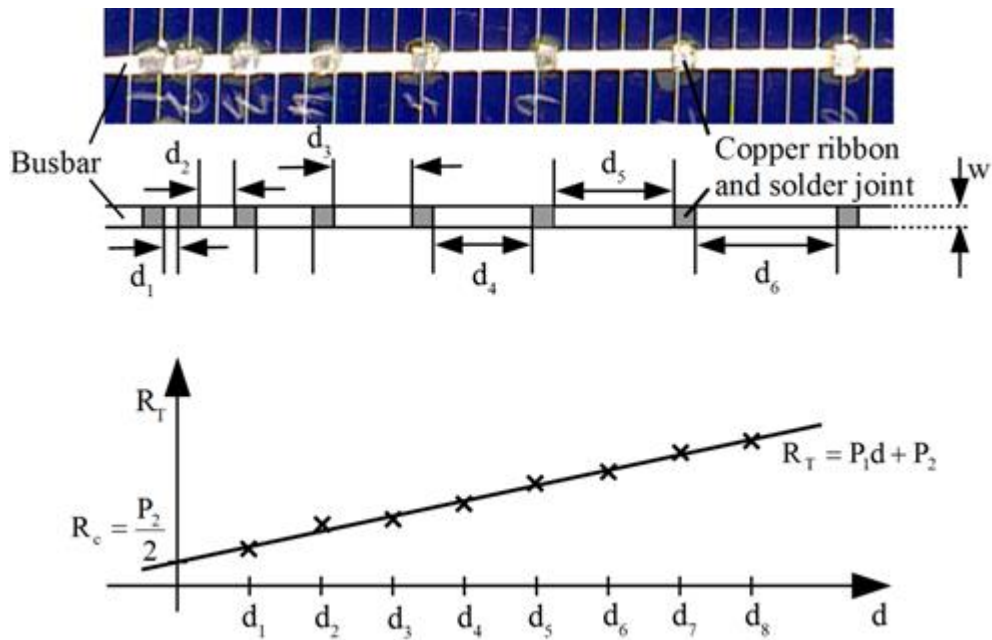


**Figure 3.16: Illustration of the Solder Joints Resistance Measurement Procedure**

The values of total contact resistance,  $R_T$  for all sections with different value of distance between two solder joints,  $d$  can be plotted and linear equation of  $R_T = P_1d + P_2$  is inserted into the curve as illustrated in Figure 3.16. By comparing the Equation 3.4 below with linear equation shown in Figure 3.16,

$$R_T = \frac{R_{busbar}}{W}d + 2R_c \quad (3.4)$$

where,

$R_{busbar}$  = Resistance per unit square of the busbar ( $\Omega$ /square);

$R_c$  = Effective solder contact resistance under the copper ribbon ( $\Omega$ );

$d$  = Distance between copper ribbons (m);

$W$  = Width of the busbar (m)

The values of  $R_c$  and  $R_{busbar}$  can be calculated by Equation 3.5 and Equation 3.6 respectively from the value of  $P_1$  and  $P_2$ .

$$R_c = \frac{P_2}{2} \quad (3.5)$$

$$R_{busbar} = P_1 W \quad (3.6)$$

The transfer length,  $L_T$  can be calculated by solving the empirical formula for the effective solder contact resistance in Equation 3.7 below using Matlab.

$$R_C = \frac{R_{busbar} L_T}{W} \coth\left(\frac{L}{L_T}\right) \quad (3.7)$$

where,

$L_T$  = Transfer length of the solder contact (m);

$L$  = Length of the copper ribbon/solder contact (m)

Lastly, the specific solder contact resistivity,  $\rho_{solder}$  for each solar cells can be calculated by using Equation 3.8 below.

$$\rho_{solder} = R_{busbar} L_T^2 \quad (3.8)$$

where,

$\rho_{solder}$  = Specific solder contact resistivity ( $\Omega \cdot m^2$ )

## CHAPTER 4

### RESULTS AND DISCUSSION

#### 4.1 Microstructure of SAC and SAC-0.40Pt Solder Solar Sandwich Structure

The solar sandwich is made up of Pb coated Cu ribbon, solar cell with the solder paste in between. Therefore, the solar sandwich will be categorised into three parts, which are the Pb coated Cu ribbon on the top layer, the solar cell at the bottom layer and the solder paste is sandwiched between the Pb coated Cu ribbon and solar cell. Figure 4.1A and Figure 4.1B shows the sandwich structure for solders: (A) SAC and (B) SAC-0.40Pt. From Figure 4.1A, the solar sandwich is made up of the IMC layer, Ag busbar from solar cell and SAC solder paste. For Figure 4.1B, the solar sandwich is made up of IMC layer, Ag busbar from solar cell and SAC-0.40Pt solder paste.

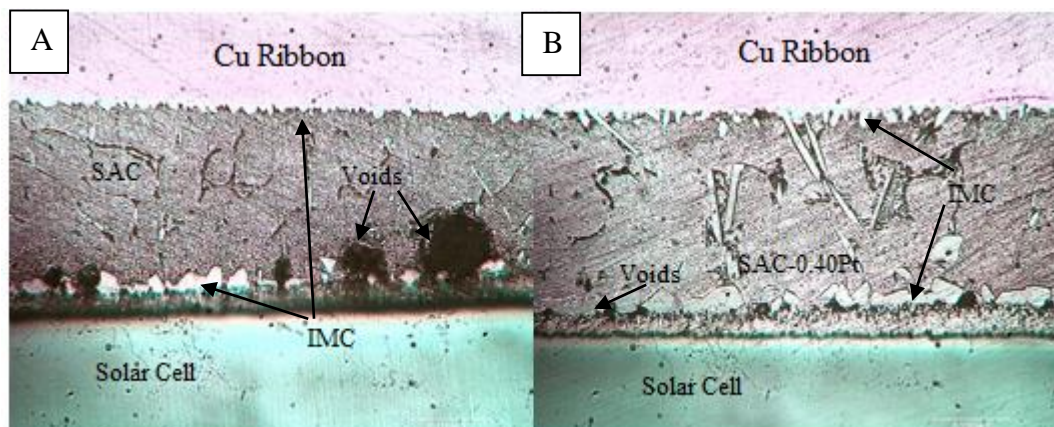


**Figure 4.1: Optical Micrograph for (A) SAC and (B) SAC-0.40Pt Solder Solar Sandwich**

The main difference between the SAC and SAC-0.40Pt samples are the amount of voids present. The hollow areas shown in the micrograph below are known as Kirkendall voids. Kirkendall voids would form is due to different vacancy concentrations during the interdiffusion process. It is also known as difference in the diffusion rates of the metal atoms, assuming all the atoms in the solder paste diffused by a vacancy mechanism. Voids form when the total outgoing atomic flux is greater than the total incoming atomic flux for the atom within a controlled volume system. Besides that, when the vacancy concentration is higher than a certain critical value for the nucleation of the voids to occur, the voids would occur during the process. Other than that, the impurities and crystal imperfections from the Cu ribbon would also assisting in the void nucleation. These impurities and imperfections would serve as heterogeneous nucleation sites for void nucleation, thus lowering the critical vacancy concentration value. Thus, the nucleation of voids would occur more easily (Y.W. Wang & Y.W. Lin, 2008). The Kirkendall void might also form when there is an insufficient solder amount, excessive amount of flux, humidity in the flux or incorrect soldering temperature and insufficient wetting between copper ribbon and busbar of solar cell (Schmitt et al., 2011).

The Kirkendall voids forming at the IMC layer would significantly reduce the total contact area between the Cu ribbon and busbar of the solar cell with the solder paste. Besides that, the voids would act as stress concentrators which causes the mechanical attachment between the solar cells, solder paste and Cu ribbon interfaces to be brittle and weaken. The excess amount of the Kirkendall voids in the solder paste region is likely to increase the brittle interfacial fracture and limit the flow of the electricity through the solder joint. Therefore, electrical conductivity of the solar cells containing many Kirkendall voids would be reduced. Lastly, the presence of Kirkendall voids may also increase the working temperature of the device. When the temperature increases, the thermal resistance of the device also increases causing the degradation due to heat dissipation of the device. All this factors will cause the efficiency of the solar cell to be lowered (Calabrese et al., 2014).

From Figure 4.1A and 4.1B, it can be observed that the amount of voids in SAC solder paste are much more than SAC-0.40Pt solder paste. This is because the Pt reinforcement in the SAC solder paste would reduce the formation of the Kirkendall

voids during the solder reflowing process. Amagai (2008) reported that, Kirkendall voids under the IMC layer can be reduced by adding Ni, Co or Pt.

Figure 4.2 shows the EDX analysis of the IMC layer formed between the Pb coated Cu ribbon and SAC solder paste. Figure 4.3 shows the EDX analysis and the elemental composition of the IMC layer formed between the busbar of bi-facial solar cell and SAC solder paste.

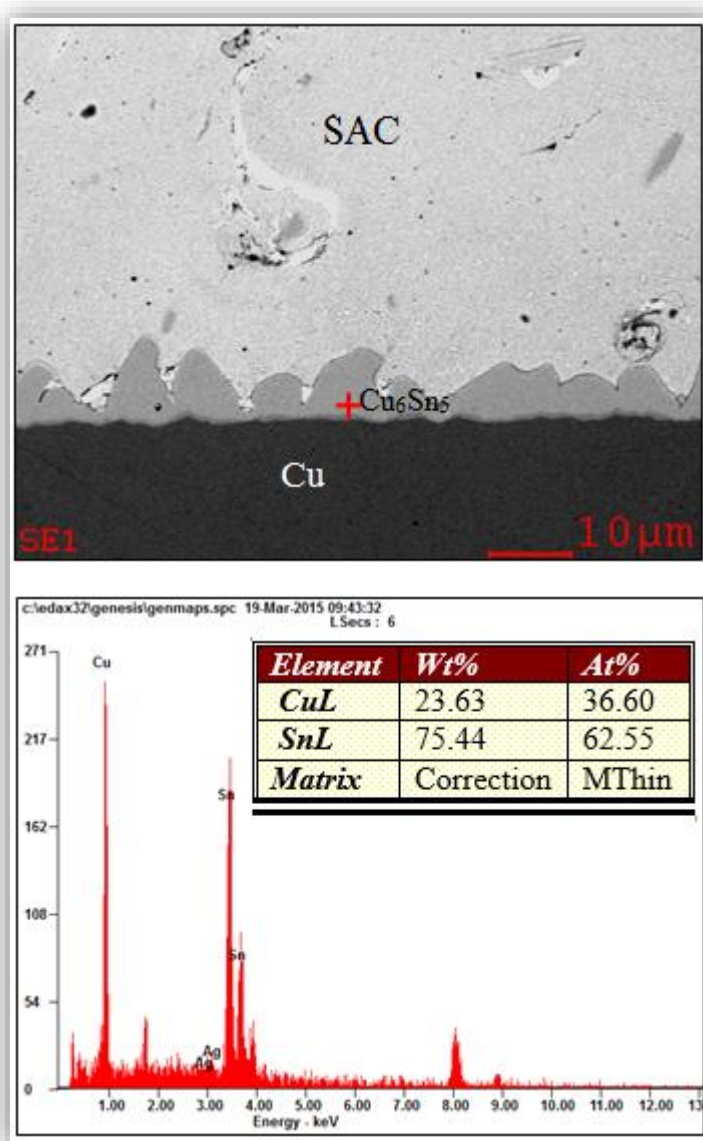


**Figure 4.2: EDX Spectroscopy Spectrums and Elemental Composition Analysis for the IMC Layer Formed between the Interface of SAC Solder and the Pb Coated Cu Ribbon**

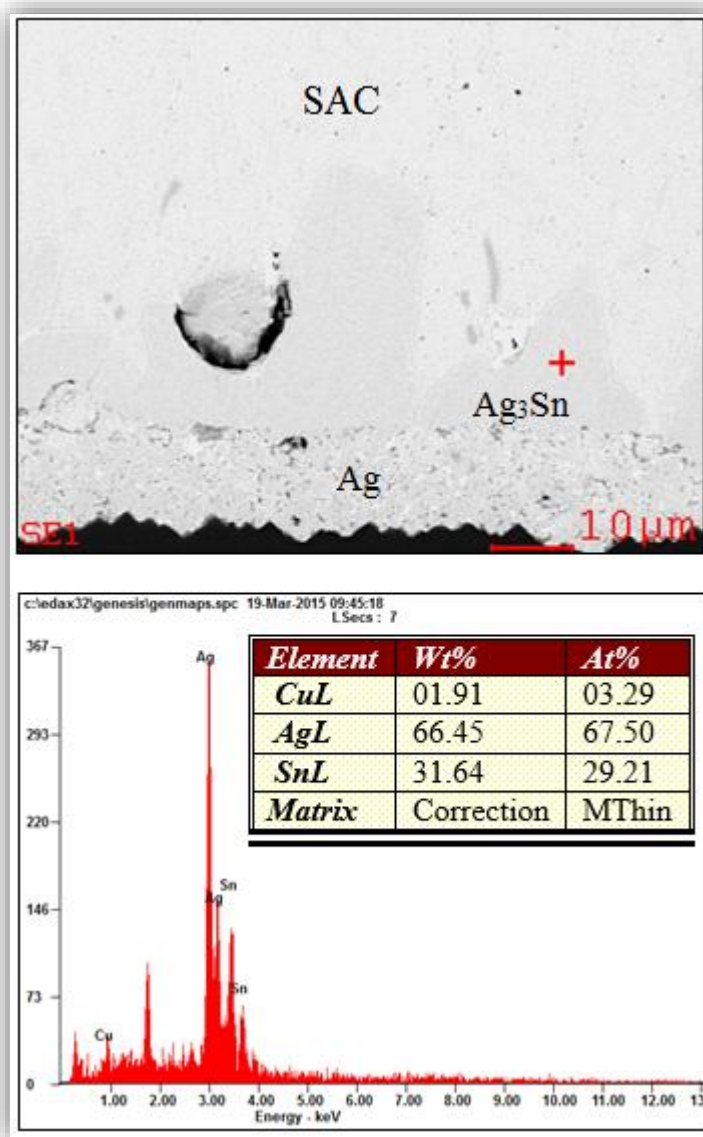


**Figure 4.3: EDX Spectroscopy Spectrums and Elemental Composition Analysis for the IMC Layer Formed between the Interface of SAC Solder and the Ag Busbar of Bi-facial Solar Cell**

From Figure 4.2 and Figure 4.3, sharp and uneven scalloped-shaped IMC layer structures are formed at the Cu ribbon/solder and Ag busbar/solder interface of the solar sandwich in the samples without Pt reinforcement. The Cu<sub>6</sub>Sn<sub>5</sub> IMC layer is formed at the interface between SAC solder and the Pb coated Cu ribbon. The Ag<sub>3</sub>Sn IMC layer is formed at the interface between SAC solder and the Ag busbar of the bi-facial solar cell. The Ag<sub>3</sub>Sn IMC layer thickness is thicker than the Cu<sub>6</sub>Sn<sub>5</sub> IMC layer (Figure 4.2).

Figure 4.4 shows the  $\text{Cu}_6\text{Sn}_5$  IMC layer is also formed between the Pb coated Cu ribbon and SAC-0.40Pt solder paste. From the EDX result, it shows that Pt is present in the  $\text{Cu}_6\text{Sn}_5$  IMC layer when the solder paste is reinforced with 0.40 wt.% Pt. The  $\text{Ag}_3\text{Sn}$  IMC layer is also formed at the interface between the Ag busbar of the bi-facial solar cell and SAC-0.40Pt solder as shown in Figure 4.5.

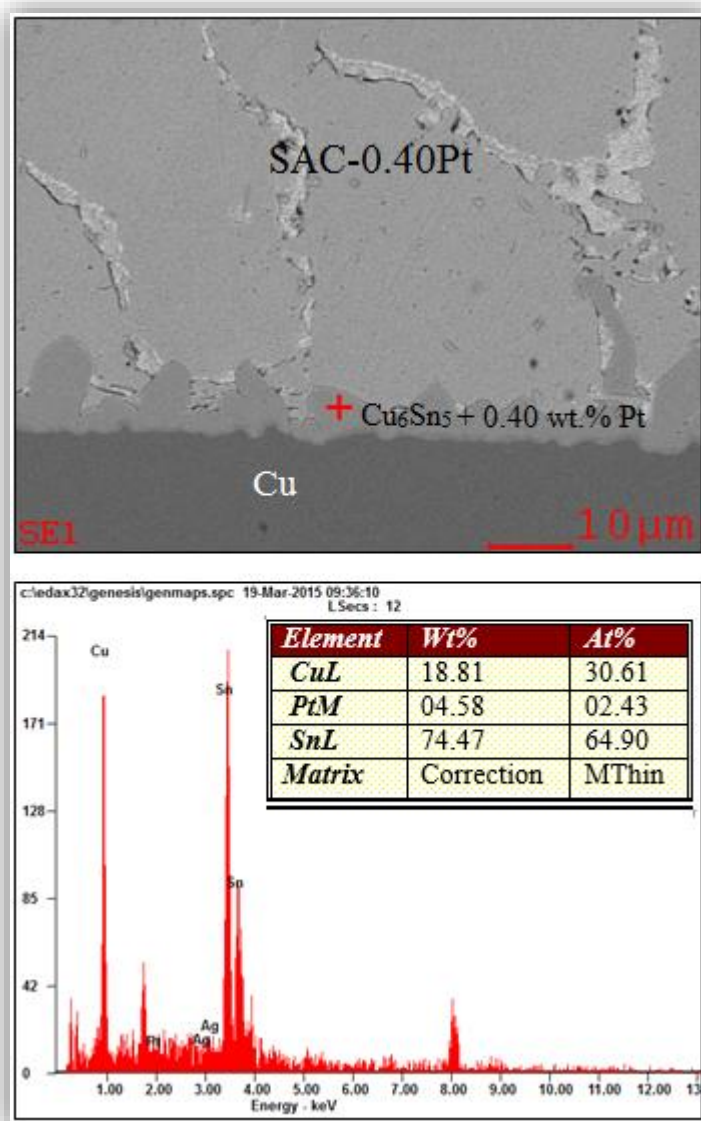


**Figure 4.4: EDX Spectroscopy Spectrums and Elemental Composition Analysis for the IMC Layer Formed between the Interface of SAC-0.40Pt Solder and the Pb Coated Cu Ribbon**

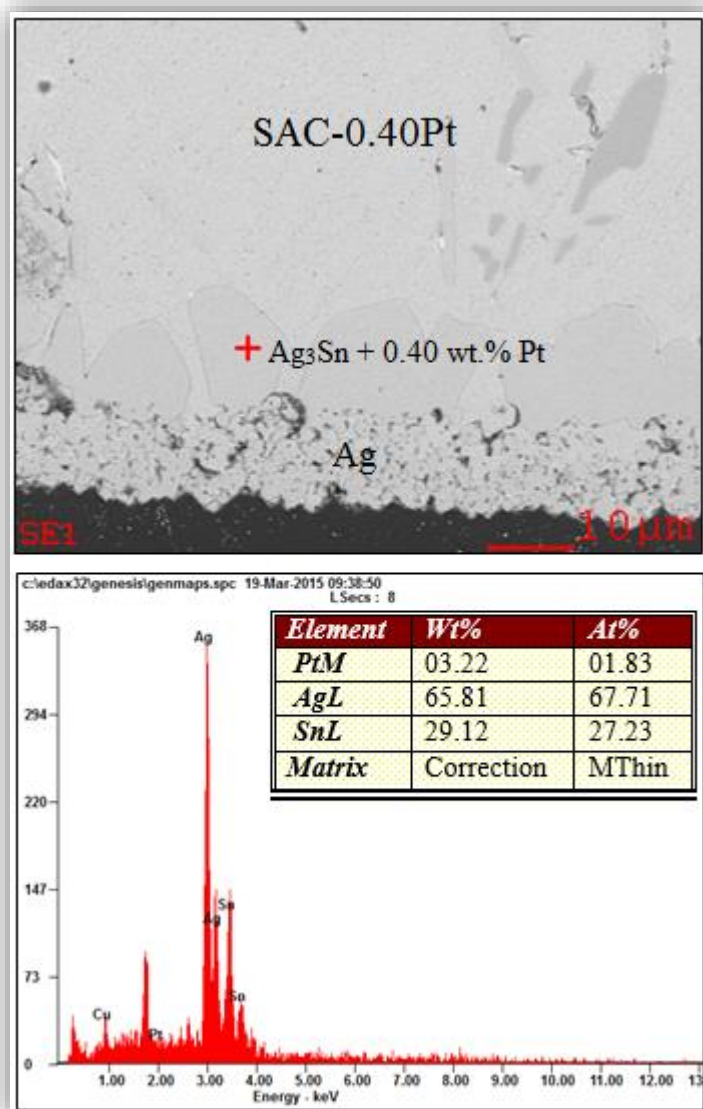


**Figure 4.5: EDX Spectroscopy Spectrums and Elemental Composition Analysis for the IMC Formed between the Interface of SAC-0.40Pt Solder and the Ag Busbar of Bi-facial Solar Cell**

The smooth and more evenly distributed  $\text{Cu}_6\text{Sn}_5$  IMC layer structure is formed at the interface between SAC-0.40Pt solder and the Pb coated Cu ribbon (Figure 4.4). The  $\text{Ag}_3\text{Sn}$  IMC layer is formed at the interface between SAC-0.40Pt solder and the Ag busbar of the bi-facial solar cell (Figure 4.5).

By comparing the IMC layers for SAC and SAC-0.40Pt solder in Figure 4.2 to Figure 4.5, it is obvious that the  $\text{Cu}_6\text{Sn}_5$  IMC layer in Figure 4.4 is more even compared

to the  $\text{Cu}_6\text{Sn}_5$  IMC layer in Figure 4.2. For the  $\text{Ag}_3\text{Sn}$  IMC layer in Figure 4.5 has more rounded rectangular edges and continuous compared with the  $\text{Ag}_3\text{Sn}$  IMC layer in Figure 4.3.

Pb is present in the solder region as shown in Figure 4.6. This is because the Pb coated-ribbon dissolved into the solder paste during reflow soldering. Pb appears as bright silver when viewed under the SEM.

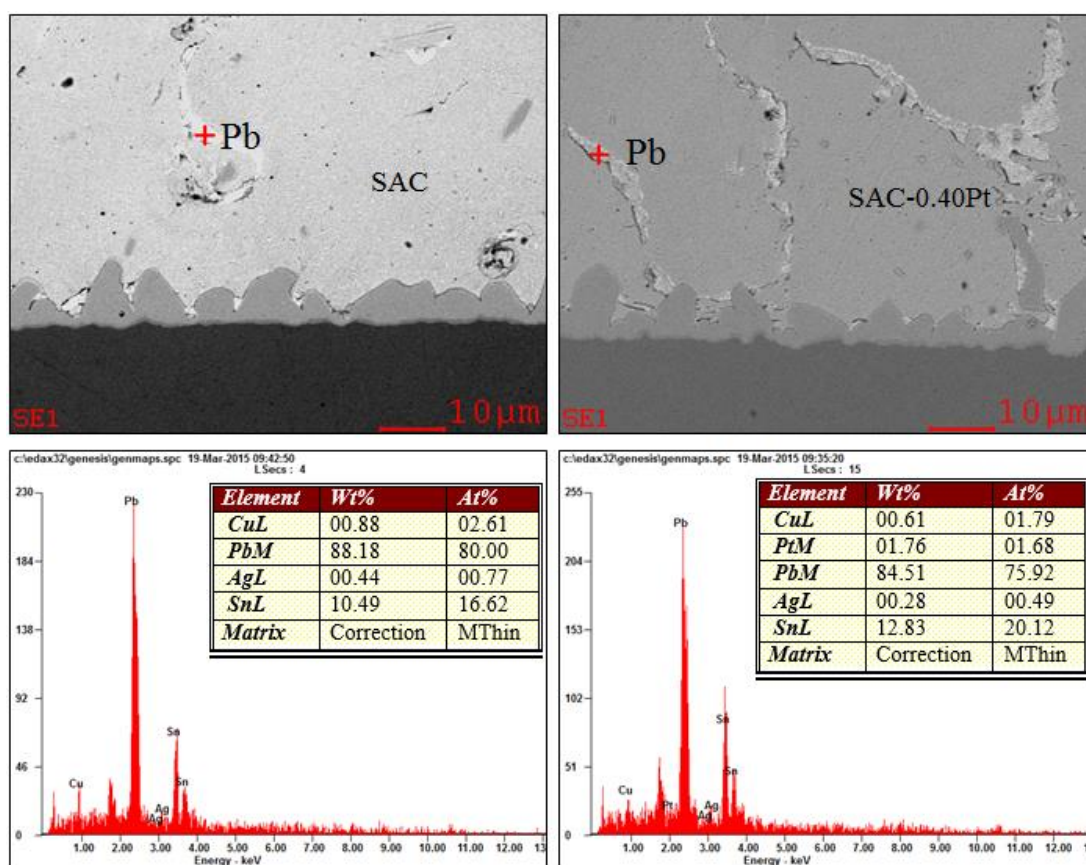


**Figure 4.6: EDX Spectroscopy Spectrums and Elemental Composition Analysis for the Pb Element on the Solder Paste Region**

Figure 4.7 shows the  $\text{Cu}_6\text{Sn}_5$  IMC layer at the solder-ribbon interface of solar sandwich with SAC and SAC-0.40Pt solder paste. Micrograph A in Figure 4.7 is the microstructure of solar sandwich with SAC solder paste without Pt reinforcement. Micrograph B is the microstructure of solar sandwich with SAC solder paste with 0.40 wt.% of platinum reinforcement. The  $\text{Cu}_6\text{Sn}_5$  IMC layer in micrograph A is unevenly distributed along the copper ribbon interface and with more thick and spiky

compounds growing above the scalloped layer. The spiky structures present will act as stress concentrators which reduces the joint reliability. The  $\text{Cu}_6\text{Sn}_5$  IMC layer in micrograph B is more evenly distributed.

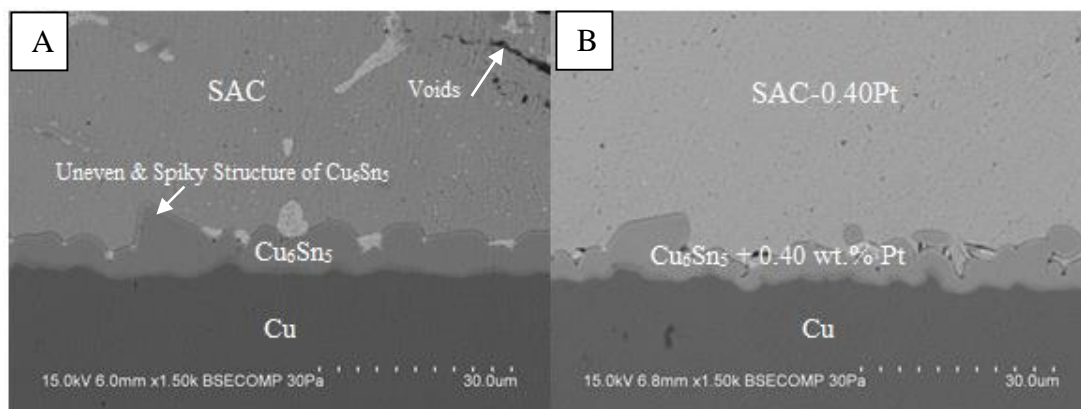


**Figure 4.7: SEM Micrographs at Solder-Ribbon Interface of Solar Sandwich**

The average thickness of IMC for the  $\text{Cu}_6\text{Sn}_5$  layer in SAC solder paste was calculated as shown in Figure 4.8 and Table 4.1.

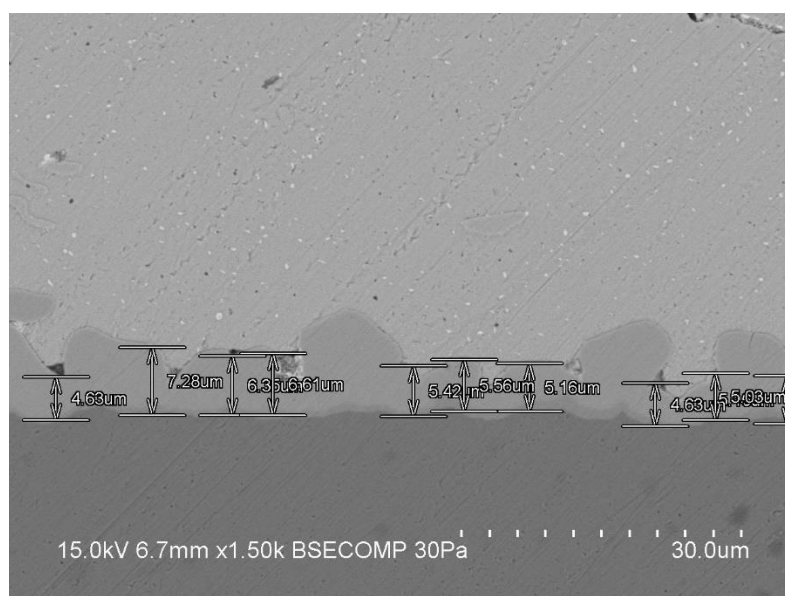


**Figure 4.8: IMC Thickness Measurements of the  $\text{Cu}_6\text{Sn}_5$  Layer Formed at the SAC Solder-Ribbon Interface**

**Table 4.1: IMC Thickness of the Cu<sub>6</sub>Sn<sub>5</sub> Layer Formed at the SAC Solder-Ribbon Interface**

No. of IMC Thickness	Thickness (μm)
1	4.63
2	7.28
3	6.36
4	6.61
5	5.42
6	5.56
7	5.16
8	4.63
9	5.43
10	5.03
<b>Average Thickness</b>	<b>5.61</b>

Figure 4.9 and Table 4.2 are used to calculate the average of IMC thickness of Cu<sub>6</sub>Sn<sub>5</sub> layer at the SAC-0.40Pt solder-ribbon interface.

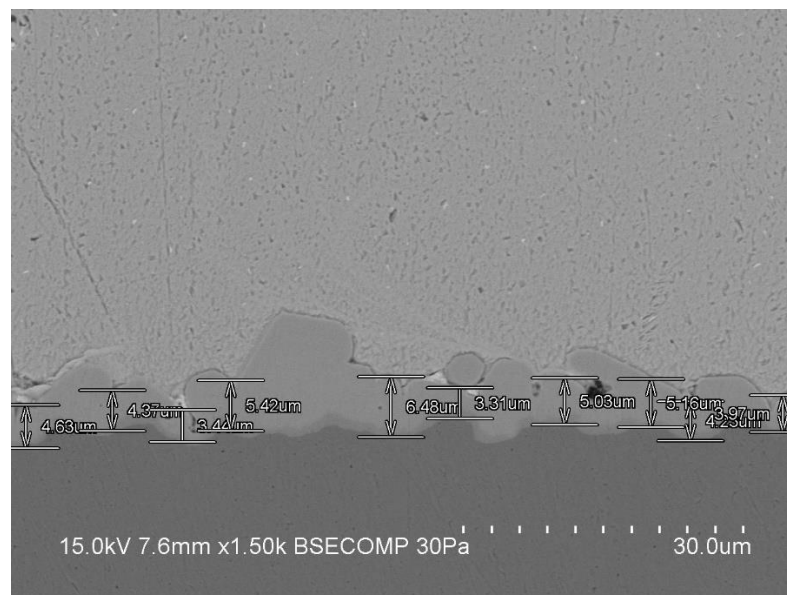


**Figure 4.9: IMC Thickness Measurements of the Cu<sub>6</sub>Sn<sub>5</sub> Layer Formed at the SAC-0.40Pt Solder-Ribbon Interface**

**Table 4.2: IMC Thickness of the Cu<sub>6</sub>Sn<sub>5</sub> Layer Formed at the SAC-0.40Pt Solder-Ribbon Interface**

<b>No. of IMC Thickness</b>	<b>Thickness (μm)</b>
1	4.63
2	4.37
3	3.40
4	5.42
5	6.48
6	3.31
7	5.03
8	5.16
9	4.03
10	3.97
<b>Average Thickness</b>	<b>4.52</b>

The Cu<sub>6</sub>Sn<sub>5</sub> IMC layer thickness for the solder alloy without platinum reinforcement is greater than that in the 0.40 wt.% Pt sample. The average IMC layer thickness for solder alloy without platinum is 5.61 μm, while the Pt containing sample has IMC layer thickness of 4.52 μm. This means that there is a reduction in IMC layer thickness by 19.43%. Pt has a lower dissolution rate compared to Cu. Presence of Pt in the solder paste would reduce solubility of Cu and slow down the Cu growth in the molten solder during reflow soldering process (Wang & Liu, 2007). This results in the Cu<sub>6</sub>Sn<sub>5</sub> IMC layer becoming more even and flat.

Figure 4.10 shows the SEM micrographs of solder-Ag busbar interface for solar sandwich with SAC and SAC-0.40Pt solder paste. The Ag<sub>3</sub>Sn IMC layer at SAC solder paste has a block-like structure at the surface of Ag busbar of the bi-facial solar cell and needles structure in the solder paste region. The Ag<sub>3</sub>Sn IMC layer in the Pt-containing sample have a flatter, evenly distributed and rounded structures. Sample without Pt show discontinuous and block-like structures (Figure 4.10A) while the Pt-containing sample have continuous layer with less gaps.

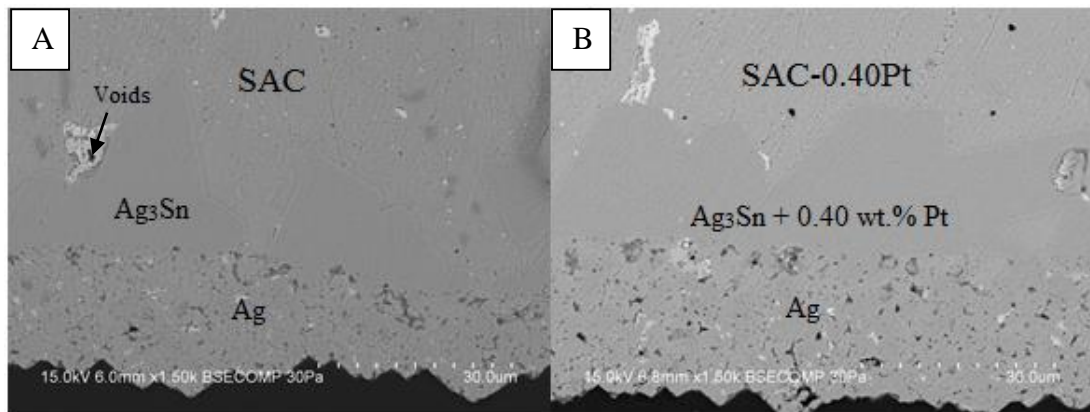


**Figure 4.10: SEM Micrographs at Solder-Ag Busbar Interface of Solar Sandwich**

## 4.2 Microstructure of Samples after Exposure Under the Sun

Figure 4.11 and Figure 4.12 shows the SEM micrographs of samples with and without Pt additions in the solar cell exposed under the sun from zero to five weeks. The IMC layer thickness is measured using the analytical programme attached to the SEM. The average IMC layer thickness for every micrographs was calculated and recorded in Table 4.5 and a graph of IMC layer thickness against times is plotted for both SAC and SAC-0.40Pt solder solar cells as shown in Figure 4.15.

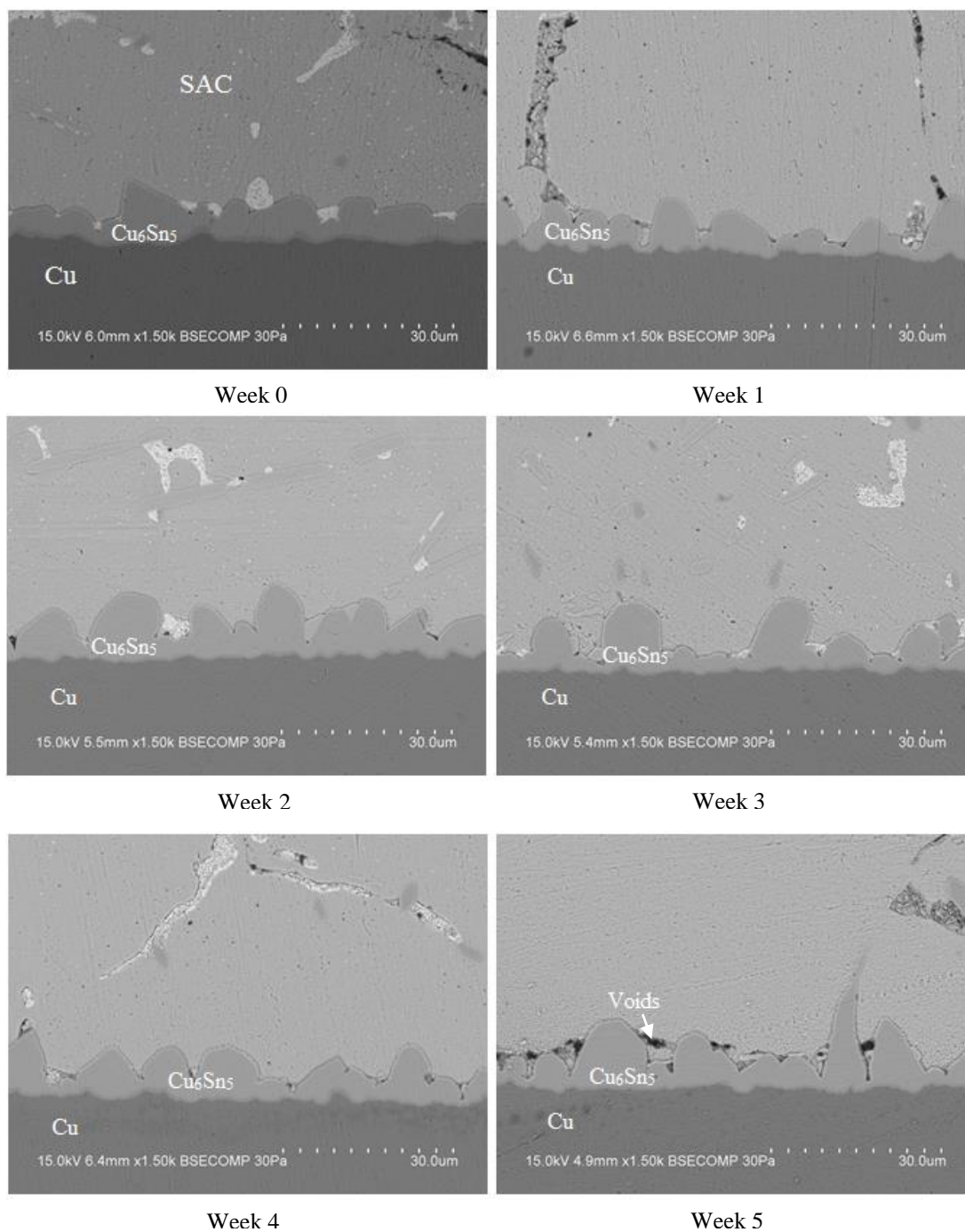


**Figure 4.11: SEM Micrographs at the Solder-Ribbon Interface for SAC Solder for Different Weeks**

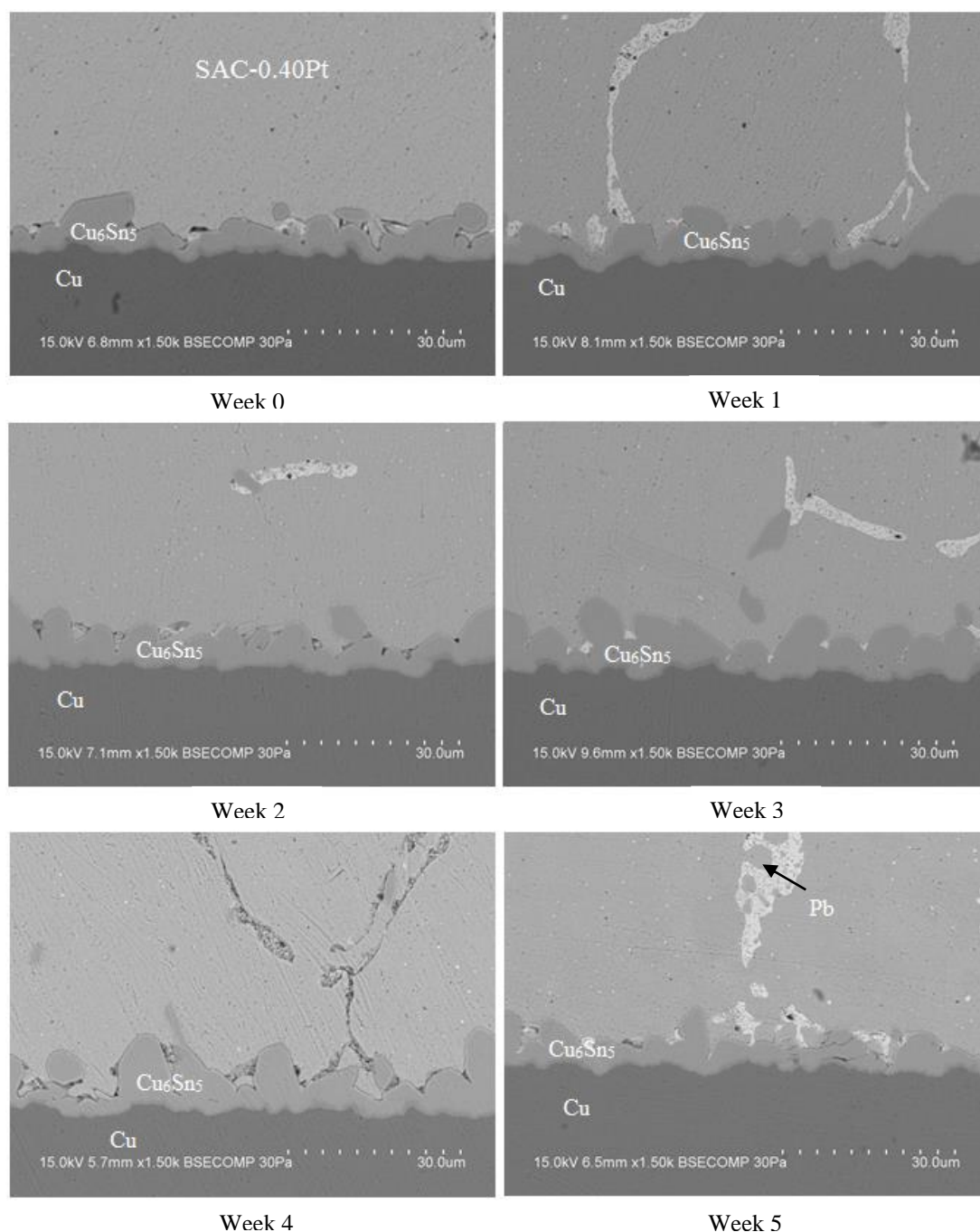


**Figure 4.12: SEM Micrographs at the Solder-Ribbon Interface for SAC-0.40Pt Solder for Different Weeks**

Figure 4.13 along with Table 4.3 was used to determine the average IMC layer thickness for the SAC sample while Figure 4.14 along with Table 4.4 was used to determine the average IMC layer thickness for the SAC-0.40Pt sample. IMC layer thickness for different exposure times are calculated in the same way.

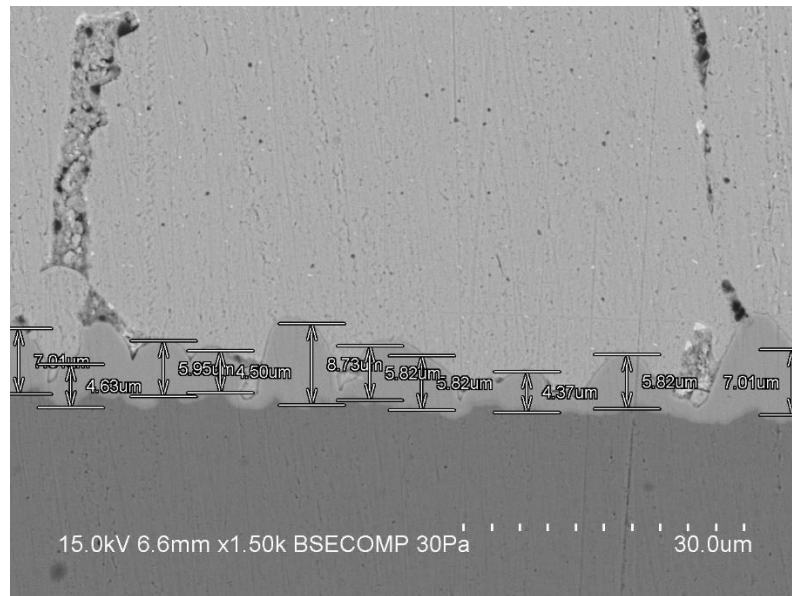


**Figure 4.13: IMC Thickness Measurements of the  $\text{Cu}_6\text{Sn}_5$  Layer Formed at the SAC Solder-Ribbon Interface (Week1)**

**Table 4.3: IMC Thickness of the  $\text{Cu}_6\text{Sn}_5$  Layer Formed at the SAC Solder-Ribbon Interface (Week 1)**

No. of IMC Thickness	Thickness ( $\mu\text{m}$ )
1	7.01
2	4.63
3	5.95
4	4.50
5	8.73
6	5.82
7	5.82
8	4.37
9	5.82
10	7.01
<b>Average Thickness</b>	<b>5.97</b>

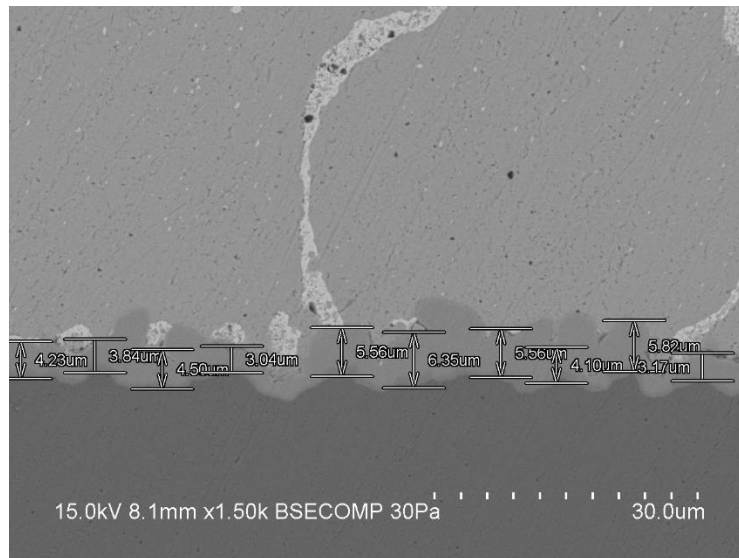


**Figure 4.14: IMC Thickness Measurements of the  $\text{Cu}_6\text{Sn}_5$  Layer Formed at the SAC-0.40Pt Solder-Ribbon Interface (Week 1)**

**Table 4.4: IMC Thickness of the  $\text{Cu}_6\text{Sn}_5$  Layer Formed at the SAC-0.40Pt Solder-Ribbon Interface (Week 1)**

No. of IMC Thickness	Thickness ( $\mu\text{m}$ )
1	4.23
2	3.84
3	4.50
4	3.04
5	5.56
6	6.35
7	5.56
8	4.10
9	5.82
10	3.17
<b>Average Thickness</b>	<b>4.62</b>

The  $\text{Cu}_6\text{Sn}_5$  IMC layer thickness increases as the exposure time under the sun increases. This is due to the growth of the IMC layer. The growth rate of IMC layer thickness layer depends on the temperature of exposure. Higher temperatures will result in higher IMC layer thickness. The Pt-reinforced solar cell has slower rate of growth for the IMC layer thickness as observed from the slope of the curve from the graph (Figure 4.15). The resistivity of the bi-facial solar cell increases as the IMC layer thickness increases due to more hindrance to the electron mobility. As a result, the performance and efficiency of the solar module would be reduced when the resistance of the solar cell increases weekly due to the growth of IMC layer thickness. Lastly, the excessive growth of IMC layer will affect thermal and structural reliability of the solder joints.

More Kirkendall voids are present in SAC sample. The Kirkendall voids increases when the exposure time at high temperature increases. Y.W. Wang & Y.W. Lin (2008) reported that the growth of  $\text{Cu}_3\text{Sn}$  IMC layer would induce the formation of Kirkendall voids, while the growth of the  $\text{Cu}_6\text{Sn}_5$  IMC layer does not. The relatively rapid diffusion of Cu out of the  $\text{Cu}_3\text{Sn}$  IMC layer could be the major contributing factor for the formation of these voids. It was shown that although both Cu and Sn were mobile within  $\text{Cu}_3\text{Sn}$  IMC layer, the Cu flux was greater than that of the Sn flux. Thus, Kirkendall voids will increase with exposure time. The formation of Kirkendall voids accompanying the  $\text{Cu}_3\text{Sn}$  IMC layer growth raises serious reliability concerns because excessive void formation increases the potential for brittle interfacial fracture. This would further increases the resistance between the conduction layers with solder, thus reduces the performance and conductivity of the solar cells. Lastly, the voids present between the Cu ribbon and solder paste tend to act as a stress concentrators which weaken the mechanical strength of the joint, in turn, affecting electrical conductivity due to impaired joints.

**Table 4.5: IMC Layer Thickness for SAC and SAC-0.40Pt Solder Solar Cells at Different Weeks**

Solder Composition	IMC Layer Thickness ( $\mu\text{m}$ )					
	Week 0	Week 1	Week 2	Week 3	Week 4	Week 5
SAC	5.61	5.97	6.54	6.90	7.32	8.09
SAC-0.40Pt	4.52	4.62	4.69	4.89	5.65	5.90

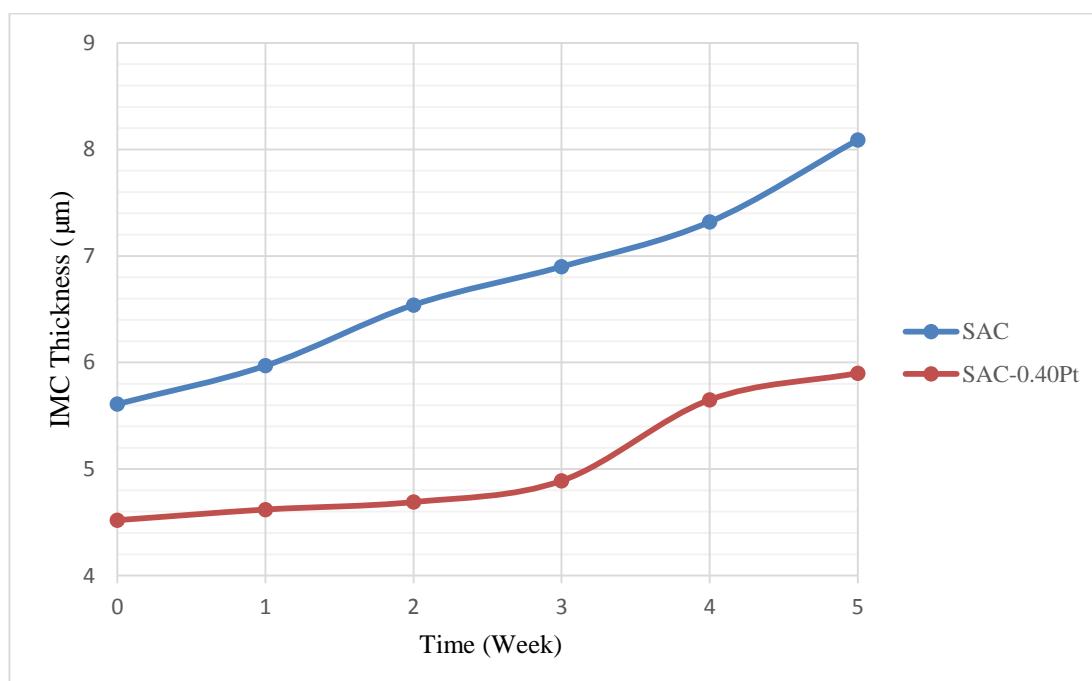


**Figure 4.15: Cu<sub>6</sub>Sn<sub>5</sub> IMC Layer Thickness for SAC and SAC-0.40Pt Solder Solar Cells at Different Weeks**

The other IMC layer at the solder-Ag busbar interface is the Ag<sub>3</sub>Sn. It is thicker compared to the Cu<sub>6</sub>Sn<sub>5</sub> IMC layer. Figure 4.16 and Figure 4.17 shows the micrographs for IMC layer of Ag<sub>3</sub>Sn at the Ag busbar surface from week 0 (without exposure) to week 5 for SAC and SAC-0.40Pt samples respectively. The Ag<sub>3</sub>Sn IMC layer is more continuous and has round edge when Pt was present in the solder paste. Besides that, the voids present in the solar sandwich reinforced with Pt is less. The number of Kirkendall voids formed increases with the solar cells exposure time increases due to the growth of Ag<sub>3</sub>Sn IMC layer.

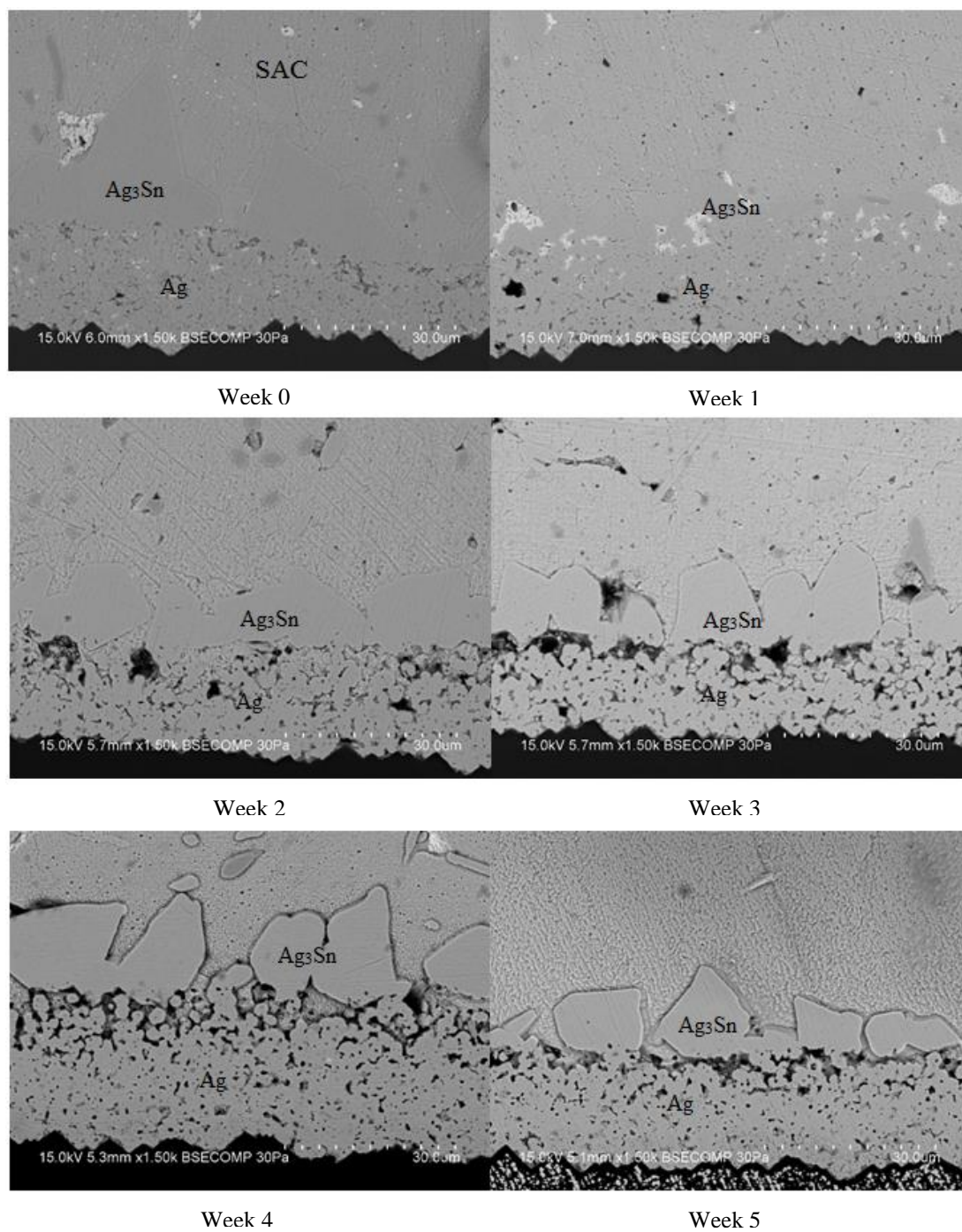


**Figure 4.16: SEM Micrographs at the Solder-Ag Busbar Interface for SAC Solder**

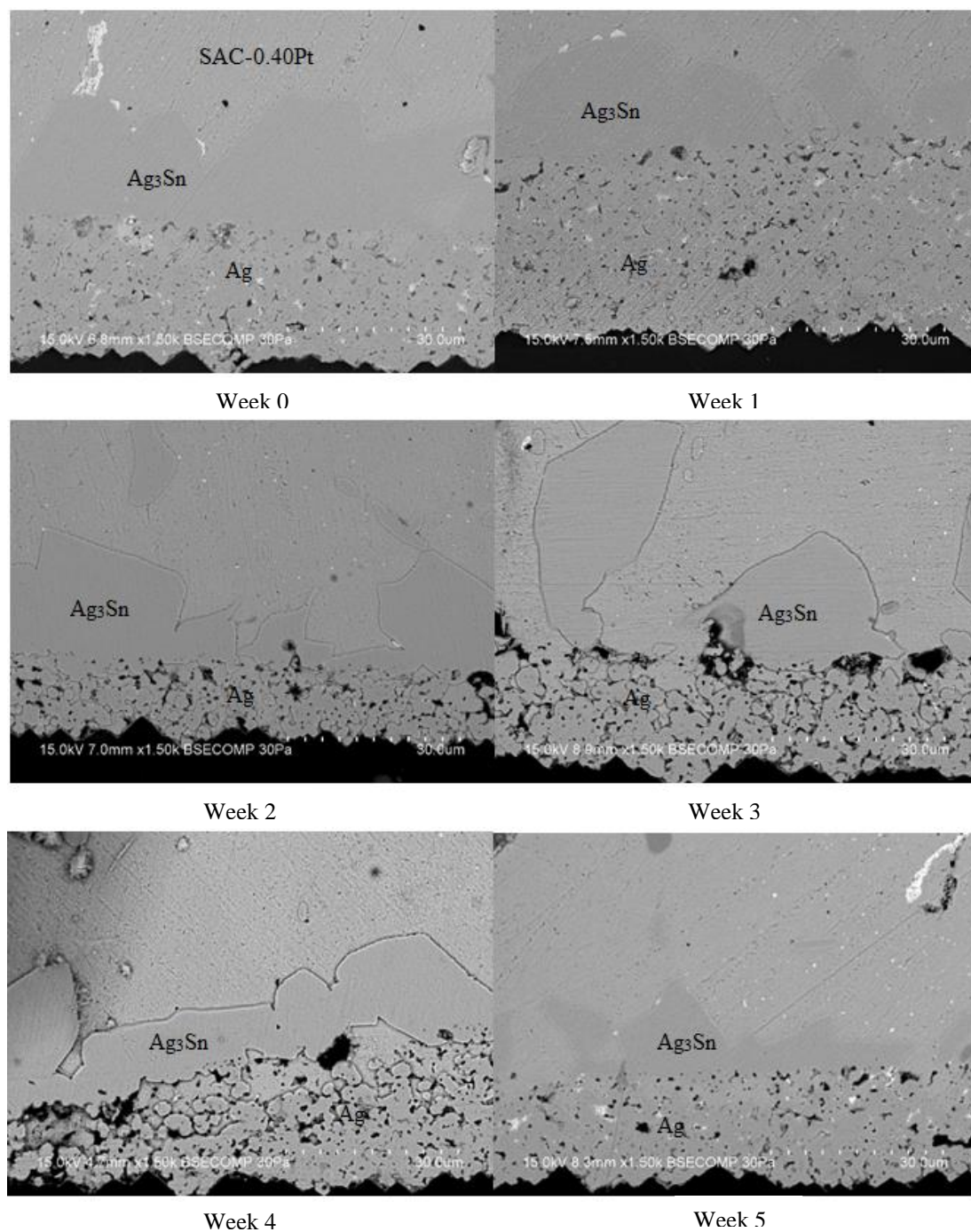


**Figure 4.17: SEM Micrographs at the Solder-Ag Busbar Interface for SAC-0.40Pt Solder**

### 4.3 Microstructure of Samples after Heat Treatment

It can be observed that the IMC layer thickness increases when the heat treatment time increases. In general, Pt-containing samples have slower IMC layer growth rate compared to SAC samples. Besides, growing rate of the IMC layer for both SAC and SAC-0.40Pt samples is higher than that of samples exposed under the sunlight. This is mainly due to the heat treatment temperature (80°C), compared to the temperature under the sunlight at approximately 35-40°C.

Based on the micrograph obtained, the number of Kirkendall voids developed in SAC solder solar cell is greater compared to SAC-0.40Pt solder solar cell after heat treatment at 80°C. The Kirkendall voids increase as the heat treatment duration increased. Besides that, the  $\text{Cu}_6\text{Sn}_5$  IMC layer in SAC solder solar cell consists of many micro-cracks. The micro-cracks are also one of the factors affecting the performance and reliability of the bi-facial solar cells. Micro-cracks in the IMC layer will reduce the structural integrity of the solder joints and disrupt the mean free path for electron movement in the solar cell thereby lowering electrical conductivity.

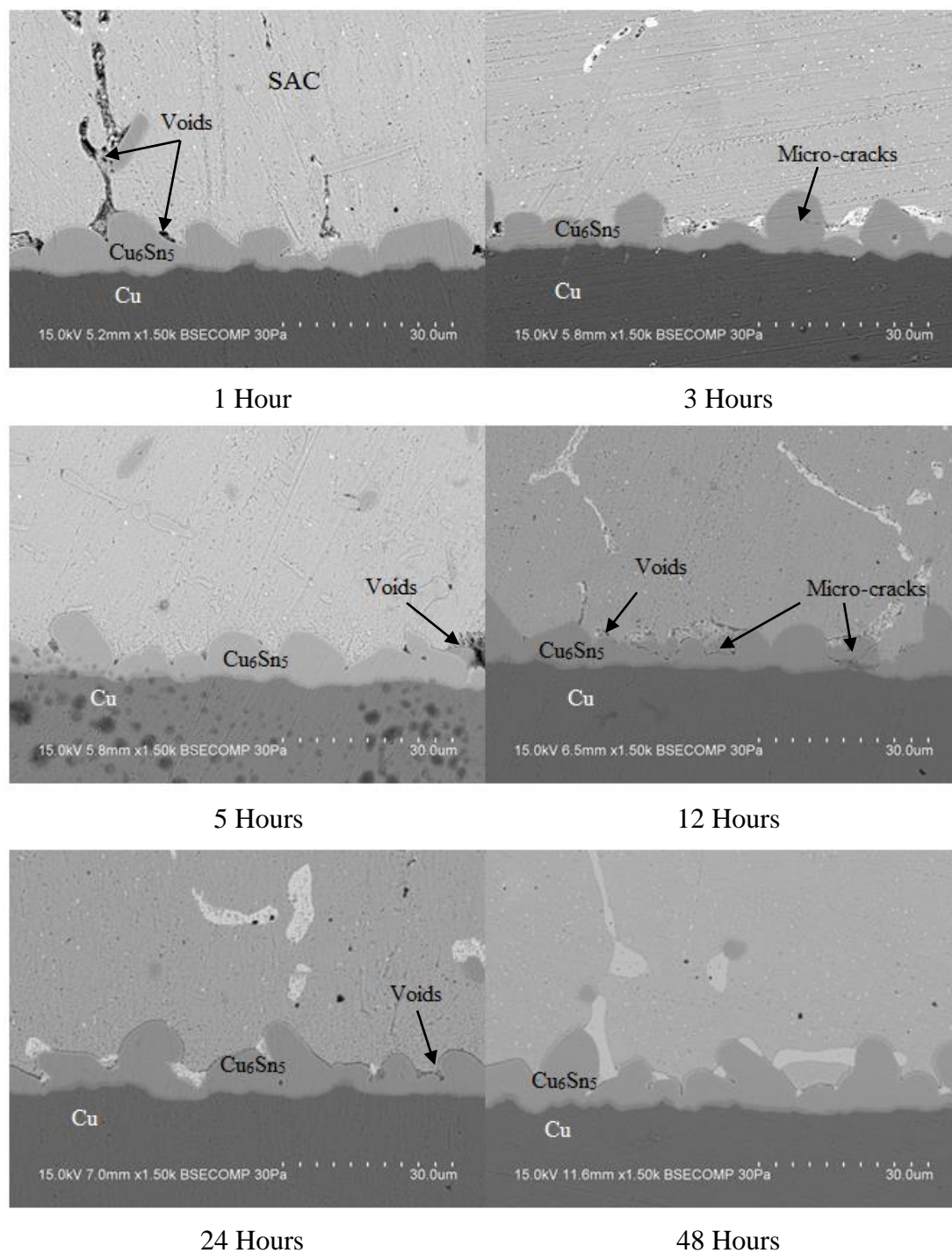


**Figure 4.18: SEM Micrographs at the Solder-Ribbon Interface for SAC Solder after Different Periods of Heat Treatment**

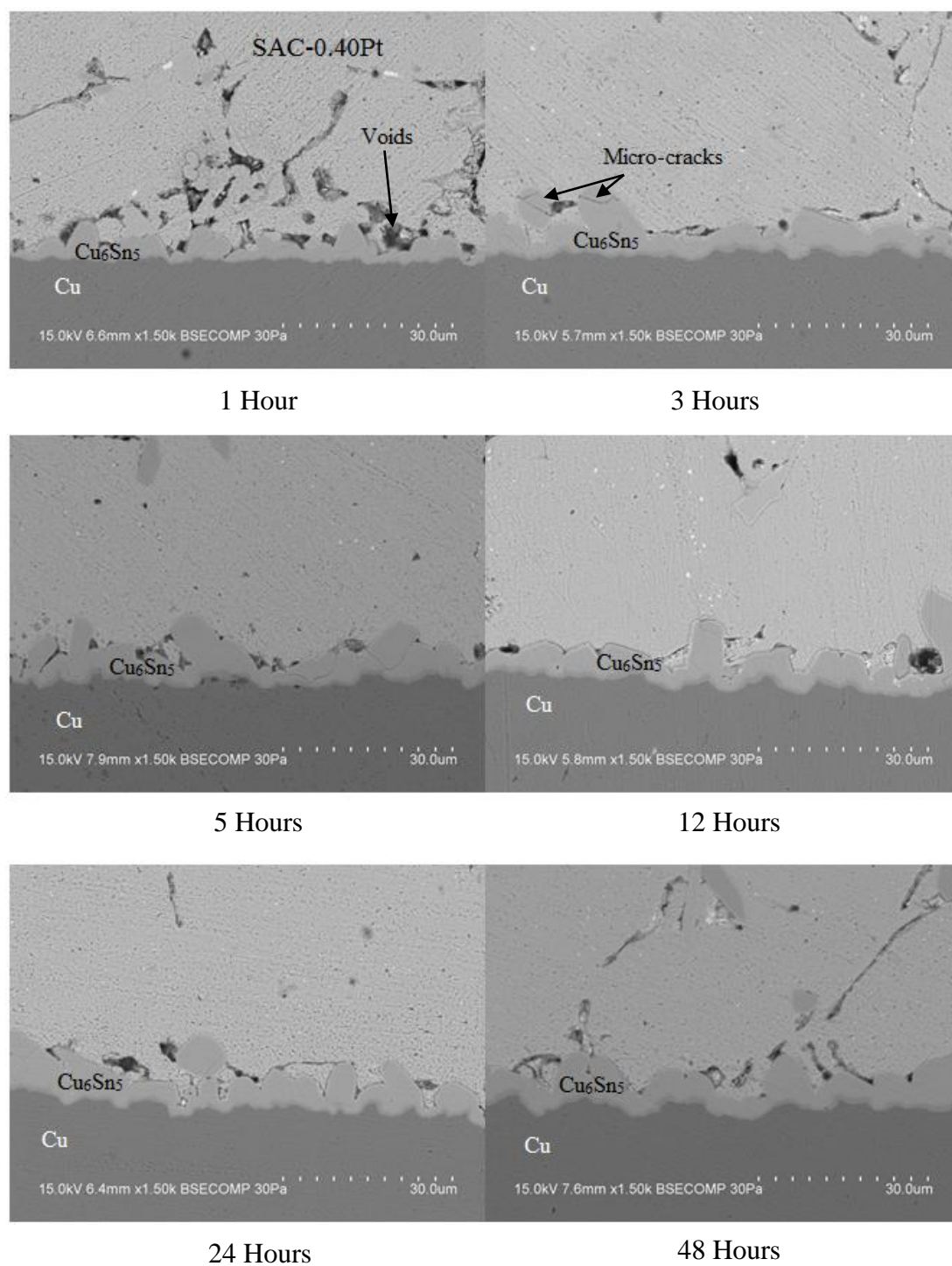


**Figure 4.19: SEM Micrographs at the Solder-Ribbon Interface for SAC-0.40Pt Solder after Different Periods of Heat Treatment**

**Table 4.6: IMC Layer Thickness for SAC and SAC-0.40Pt Solder Solar Cells for Different Heat Treatment Times**

Solder Composition	IMC Layer Thickness ( $\mu\text{m}$ )					
	1 hours	3 hours	5 hours	12 hours	24 hours	48 hours
SAC	5.82	6.47	7.15	7.40	8.65	8.96
SAC-0.40Pt	4.90	5.47	5.67	5.85	6.19	6.48

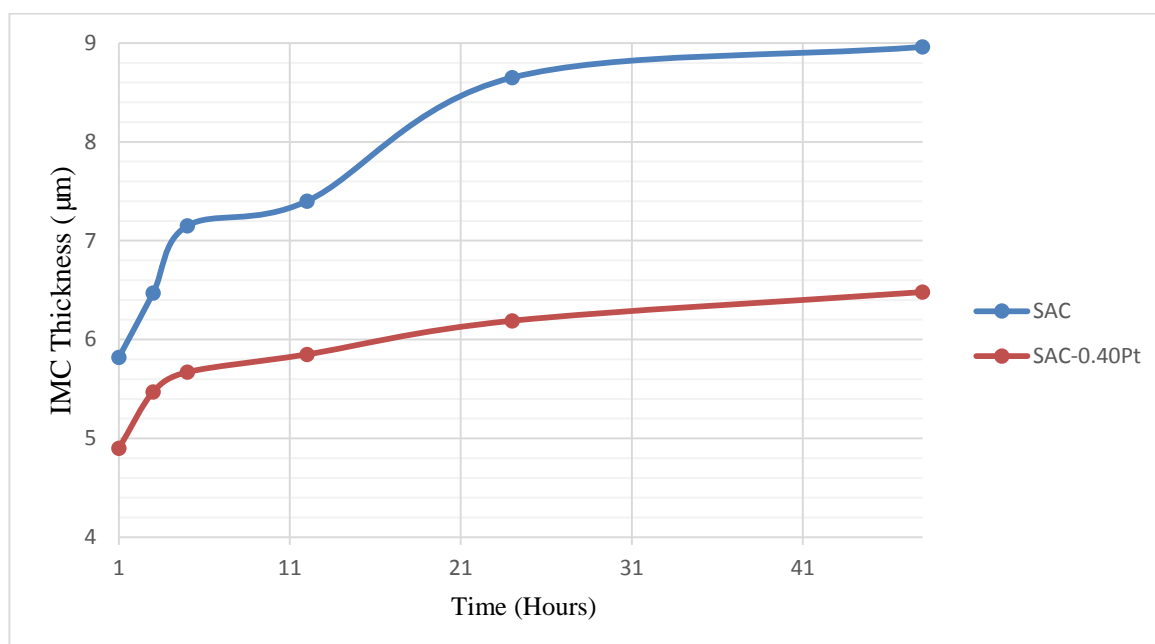


**Figure 4.20:  $\text{Cu}_6\text{Sn}_5$  IMC layer Thickness for SAC and SAC-0.40Pt Solder for Different Heat Treatment Times**

Figure 4.21 and Figure 4.22 shows micrographs at the solder/Ag busbar metallization interface after heat treatment for various times for SAC and SAC-0.40Pt samples respectively. Comparing the two sets of samples, the Pt-containing sample have rounder and smoother IMC layer structure.

$\text{Ag}_3\text{Sn}$  IMC layer is formed at the beginning of the eutectic reaction. The primary driving force of the growth of  $\text{Ag}_3\text{Sn}$  IMC phase is due to the degree of undercooling after reflow soldering. During the solidification process, the bulk of  $\text{Ag}_3\text{Sn}$  IMC experienced minimal degree of undercooling. As such, the solar cells

exposed to sunlight and also heat treatment will not display excessive increase of the  $\text{Ag}_3\text{Sn}$  IMC layer thickness (Schmitt et al., 2012).

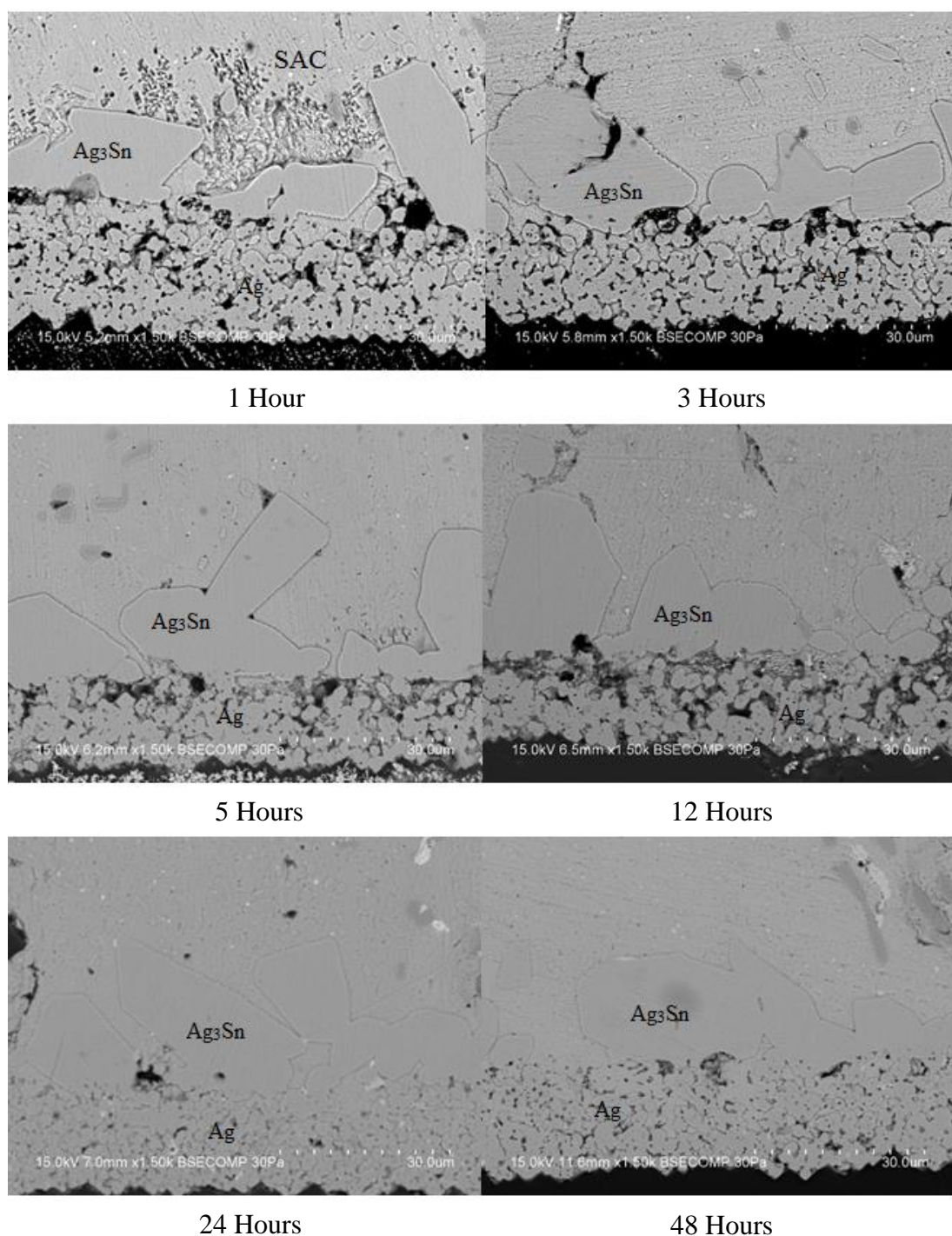


**Figure 4.21: SEM Micrographs at the Solder-Ag Busbar Interface for SAC Solder after Different Periods of Heat Treatment**

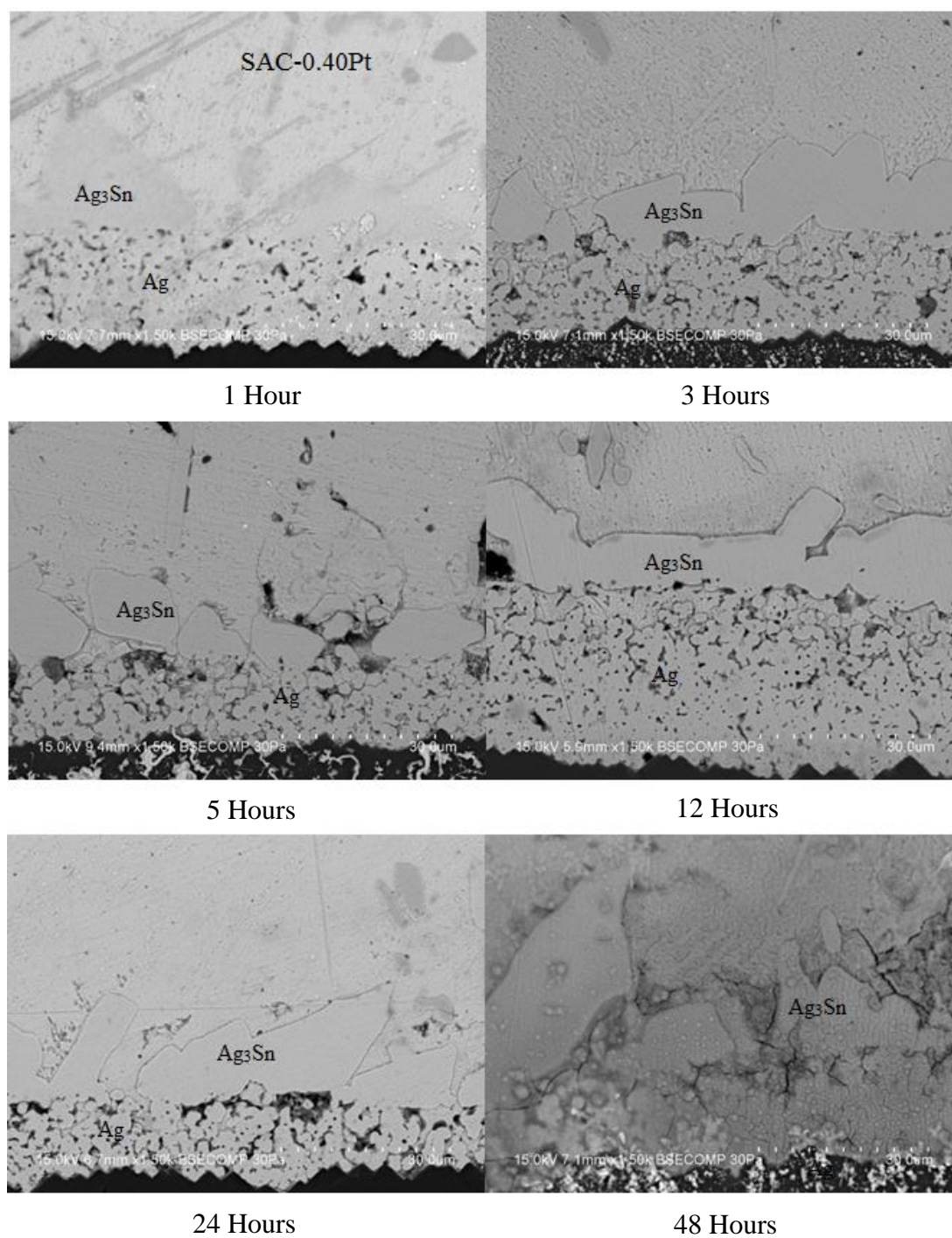


**Figure 4.22: SEM Micrographs at the Solder-Ag Busbar Interface for SAC-0.40Pt Solder after Different Periods of Heat Treatment**

#### 4.4 Resistivity of Samples after Heat Treatment

From microstructural studies, it is observed that number of Kirkendall voids and IMC layer thickness increases when exposed to sunlight or undergo heat treatment. As the voids and IMC layer develop in the solder, it is expected that the electricity conductivity of the solar cells would decrease.

Voltage is measured for each pair of solder joint using high sensitivity multimeter. The total contact resistance of the each points can then be calculated using Ohm's law.

##### Sample Calculation:

By using SAC solder solar cell without heat treatment as a sample. The resistivity at point 1 is calculated by using constant current of 98.4 mA and measured voltage of 0.239 mV. The sample calculation is shown in the below.

$$\text{Ohm's Law, } V = IR$$

$$\text{Rearrange: } R = \frac{V}{I}$$

$$R = \frac{0.239\text{mV}}{98.4\text{mA}}$$

$$R = 0.00243 \Omega$$

The calculated resistance is presented in a table form as shown (Table 4.7).

##### Solar Cells without Pt Reinforcement

**Table 4.7: Resistance Value for Each Point on the Bi-facial Solar Cell (Without Heat Treatment)**

Point	Current (mA)	Voltage (mV)	Resistance ( $\Omega$ )
1	98.4	0.239	0.00243
2	98.4	0.491	0.00499

3	98.4	0.802	0.00815
4	98.3	1.095	0.01114
5	98.3	1.285	0.01307
6	98.3	1.500	0.01526
7	98.3	1.770	0.01801
8	98.3	2.071	0.02107
9	98.3	2.225	0.02263
10	98.2	2.470	0.02515
11	98.2	2.860	0.02912
12	98.2	3.050	0.03106

### **Solar Cells with 0.40 wt.% Pt Reinforcement**

**Table 4.8: Resistance Value for Each Point on the Bi-facial Solar Cell (Without Heat Treatment)**

Point	Current (mA)	Voltage (mV)	Resistance ( $\Omega$ )
1	98.8	0.209	0.00212
2	98.8	0.435	0.00440
3	98.8	0.669	0.00677
4	98.9	0.931	0.00941
5	98.9	1.184	0.01197
6	98.9	1.359	0.01374
7	98.9	1.606	0.01624
8	99.0	1.969	0.01989
9	99.0	2.127	0.02148
10	99.0	2.316	0.02339
11	99.0	2.528	0.02554
12	99.0	2.878	0.02907

Tables for resistance of bi-facial solar cells after heat treatment for 1,3,5,12,24 and 48 hours are shown in the appendix.

Values for total contact resistance,  $R_T$  are calculated for all sections with different value of distance between two solder joints,  $d$ . The graph of total contact resistance against the different value of distance between two solder joints,  $d$  can be plotted and the linear equation of  $R_T = P_1d + P_2$  can be found on the curve as illustrated by Figure 4.23.

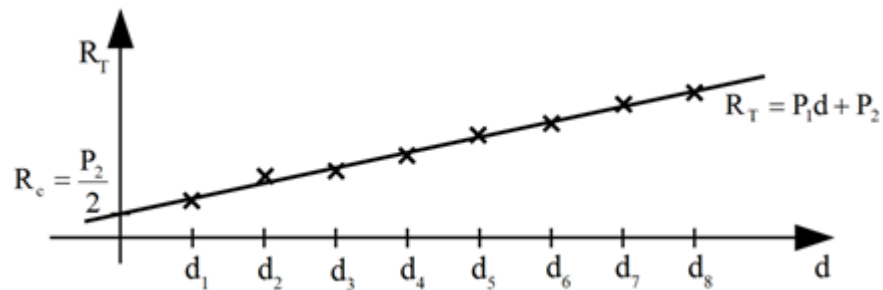


**Figure 4.23: Graph of Total Contact Resistance ( $\Omega$ ) against Distance between Two Solder Joints**

After that, the values of  $R_c$  and  $R_{busbar}$  can be calculated by Equation 4.1 and Equation 4.2 respectively from the value of  $P_1$  and  $P_2$ .

$$R_{busbar} = P_1W \quad (4.1)$$

$$R_c = \frac{P_2}{2} \quad (4.2)$$

#### Sample Calculation

By using 0.0 wt% platinum reinforced solder solar cell without heat treatment as a sample. The values of  $P_1$  and  $P_2$  from the linear equation of the graph are 1.713986  $\Omega/m$  and 0.000986  $\Omega$  respectively.

$$\begin{aligned} R_{busbar} &= (1.713986 \frac{\Omega}{m} \times 0.0015m) \\ &= 2.571 \times 10^{-3} \Omega \end{aligned}$$

where,  $W$  is 0.0015m for front side solar cell

$$R_c = \frac{0.000986 \Omega}{2}$$

$$= 4.93 \times 10^{-4} \Omega$$

The values of resistance per unit square of the busbar,  $R_{busbar}$  and effective solder contact resistance under copper ribbon,  $R_c$  for SnAgCu solder and Pt reinforced SnAgCu solder with Pt composition of 0.4 wt% were measured and calculated in the same way. The Table 4.9 and Table 4.10 shows the values of  $R_{busbar}$  and  $R_c$  for SAC and SAC-0.40Pt solder solar cells before and after heat treatment for different durations.

**Table 4.9: Summary of  $R_{busbar}$  and  $R_c$  for SAC Solder Solar Cells before and after Heat Treatment for Different Duration**

Heat Treatment Time	0 hours	1 hour	3 hours	5 hours	12 hours	24 hours	48 hours
$R_{busbar}$ ( $\Omega$ )	$2.571 \times 10^{-3}$	$2.592 \times 10^{-3}$	$2.630 \times 10^{-3}$	$2.653 \times 10^{-3}$	$2.639 \times 10^{-3}$	$2.939 \times 10^{-3}$	$3.023 \times 10^{-3}$
$R_c$ ( $\Omega$ )	$4.93 \times 10^{-4}$	$6.46 \times 10^{-4}$	$7.18 \times 10^{-4}$	$8.62 \times 10^{-4}$	$1.076 \times 10^{-3}$	$1.416 \times 10^{-3}$	$1.633 \times 10^{-3}$

**Table 4.10: Summary of  $R_{busbar}$  and  $R_c$  for SAC-0.40Pt Solder Solar Cells before and after Heat Treatment for Different Duration**

Heat Treatment Time	0 hours	1 hour	3 hours	5 hours	12 hours	24 hours	48 hours
$R_{busbar}$ ( $\Omega$ )	$2.411 \times 10^{-3}$	$2.432 \times 10^{-3}$	$2.431 \times 10^{-3}$	$2.467 \times 10^{-3}$	$2.464 \times 10^{-3}$	$2.651 \times 10^{-3}$	$2.687 \times 10^{-3}$
$R_c$ ( $\Omega$ )	$2.32 \times 10^{-4}$	$2.35 \times 10^{-4}$	$2.72 \times 10^{-4}$	$3.12 \times 10^{-4}$	$3.87 \times 10^{-4}$	$4.29 \times 10^{-4}$	$5.28 \times 10^{-4}$

In order to determine the specific solder contact resistivity,  $\rho_{solder}$  for each of the solar cells, the transfer length,  $L_T$  must first be calculated using the empirical formula for Equation 3.6 in Matlab software. The formula for specific solder contact resistivity,  $\rho_{solder}$  requires the value of transfer length,  $L_T$  as shown below.

$$\rho_{solder} = R_{busbar} L_T^2$$

where,

$\rho_{solder}$  = Specific solder contact resistivity ( $\Omega \cdot m^2$ )

Table 4.11 and Table 4.12 shows the specific solder contact resistivity values for SAC and SAC-0.40Pt solder after different heat treatment times.

**Table 4.11: Specific Solder Contact Resistivity for SAC Solder Solar Cells before and after Different Heat Treatment Duration**

Heat Treatment Time	Specific Solder Contact Resistivity ( $\Omega \cdot m^2$ )
0 hour	$2.12678 \times 10^{-10}$
1 hours	$3.61782 \times 10^{-10}$
3 hours	$4.39889 \times 10^{-10}$
5 hours	$6.24981 \times 10^{-10}$
12 hours	$9.60171 \times 10^{-10}$
24 hours	$1.45142 \times 10^{-9}$
48 hours	$1.82460 \times 10^{-9}$

**Table 4.12: Specific Solder Contact Resistivity for SAC-0.40Pt Solder Solar Cells before and after Different Heat Treatment Duration**

Heat Treatment Time	Specific Solder Contact Resistivity ( $\Omega \cdot m^2$ )
0 hour	$5.02298 \times 10^{-11}$
1 hours	$5.10922 \times 10^{-11}$
3 hours	$6.84755 \times 10^{-11}$

5 hours	$8.87814 \times 10^{-11}$
12 hours	$1.36760 \times 10^{-10}$
24 hours	$1.56120 \times 10^{-10}$
48 hours	$2.33409 \times 10^{-10}$

From Table 4.11 and Table 4.12 the percentage difference for the specific solder contact resistivity between SAC and SAC-0.40Pt solder solar cell can be calculated by using Equation 4.3. The specific solder contact resistivity of SAC solder is set as the reference value.

$$\begin{aligned} \text{Percentage Difference} &= \frac{|\text{Reference Value} - \text{Measured Value}|}{\text{Reference Value}} \times 100\% \quad (4.3) \\ \text{Percentage Difference} &= \frac{|2.12678 \times 10^{-10} - 5.02298 \times 10^{-11}|}{2.12678 \times 10^{-10}} \times 100\% \\ &= 76.38\% \end{aligned}$$

The percentage difference for specific solder contact resistivity between SAC and SAC-0.40Pt solder solar cell is 76.38%, indicating that Pt-reinforced solder paste would reduce the resistivity of the bi-facial solar cell by 76.38%. Pt particles can reduce the thickness of the IMC layer, amount of voids and micro-cracks formed.

The specific solder contact resistivity for SAC and SAC-0.40Pt solder solar cells without heat treatment act as the reference value for calculation of percentage of difference in resistivity for different heat treatment durations. The calculated values are tabulated in Table 4.13 and Table 4.14.

**Table 4.13: Percentage Difference for Specific Solder Contact Resistivity for SAC Solder Solar Cells after Different Heat Treatment Duration**

Heat Treatment Time	Percentage Difference for Specific Solder Contact Resistivity (%)
1 hour	70.11%
3 hours	106.83%

5 hours	193.86%
12 hours	351.47%
24 hours	582.45%
48 hours	757.92%

**Table 4.14: Percentage Difference for Specific Solder Contact Resistivity for SAC-0.40Pt Solder Solar Cells after Different Heat Treatment Duration**

Heat Treatment Time	Percentage Difference for Specific Solder Contact Resistivity (%)
1 hour	1.72%
3 hours	36.32%
5 hours	76.75%
12 hours	172.27%
24 hours	210.81%
48 hours	364.68%

Based on Figure 4.24, the increase of percentage difference for SAC solder solar cells after different period of heat treatment is higher compared to that of SAC-0.40Pt solder solar cells at 80°C. The rate increase for specific solder contact resistivity between SAC and SAC-0.40Pt solder solar cells can be obtained. The gradient for SAC curve is 0.3636 while that for SAC-0.40Pt curve is 0.1944. The gradient of curve for SAC solder solar cells is used as the reference value. The percentage difference for rate of increase between SAC and SAC-0.40Pt solder solar cells can be calculated as shown below.

$$\text{Percentage Difference} = \frac{|\text{Reference Value} - \text{Measured Value}|}{\text{Reference Value}} \times 100\%$$

$$\begin{aligned} \text{Percentage Difference} &= \frac{|0.1818 - 0.0972|}{0.1818} \times 100\% \\ &= 46.53\% \end{aligned}$$

Based on the calculation shown, specific solder contact resistivity during solar cells degradation will slow down by 46.53% in Pt reinforced solder solar cells. This imply that addition of Pt will improve power yield and thus efficiency of the bi-facial solar cells.

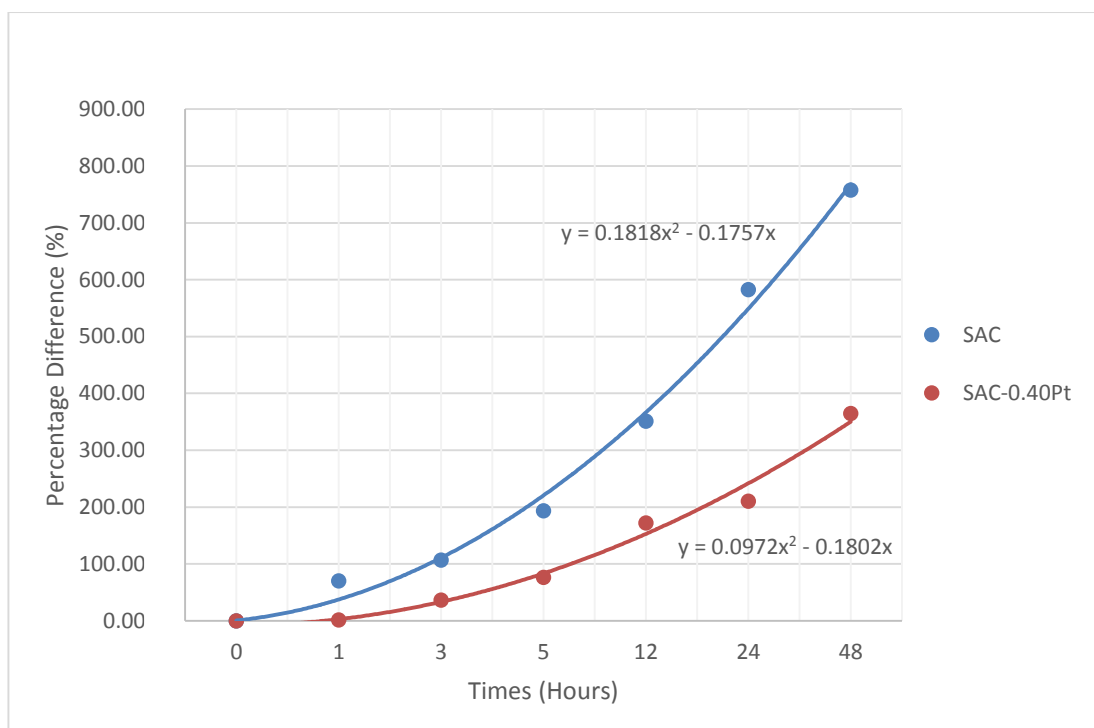


**Figure 4.24: Graph of Percentage Difference for Specific Solder Contact Resistivity (%) Versus Different Heat Treatment Duration (Hours)**

## CHAPTER 5

### CONCLUSION AND RECOMMENDATIONS

#### 5.1 Conclusion

From the result obtained, it can be conclude that:

- 1) Microstructures for samples containing 0.40 wt.% Pt in the SAC solder have less Kirkendall voids compared to those of SAC. Amounts of micro-cracks were also reduced in the Pt-containing samples.
- 2) IMC layer in Pt-containing samples are more rounded. IMC layer thickness reduced by 27.07% when 0.40 wt.% Pt was added for samples exposed under the sunlight for twenty five days. Addition of Pt is believed to reduce dissolution of Cu into the molten solder paste.
- 3) When time of exposure under the sun and also heat treatment conditions increased, the IMC layer thickness increased along with number of Kirkendall voids and micro-cracks. This is because growth of the  $\text{Cu}_6\text{Sn}_5$  IMC layer is temperature-dependent.
- 4) Resistivity of the SAC-0.40Pt sample is 76% less than that of the SAC sample. After exposure under the sunlight and also heat treatment, the resistivity increased in general.

- 5) Pt increased the conductivity of the solar cells by suppressing excessive growth of the IMC layer and the numbers of Kirkendall voids form. In turn, there are less defects in the solar sandwich structure, thus lower resistance to electron mobility, as stated by the Matthiesen's rule.

## **5.2 Recommendations**

The following recommendations are made based on observation during the project:

- 1) The temperature profile for reflow must be strictly adhered to, otherwise a proper metallurgical bonding cannot be achieved.
- 2) The Pb coated Cu ribbon should be straightened before use to avoid airtraps. This can lead to formation of voids in the solar cell.
- 3) Solder pastes have expiry dates and must be properly stored. Frequent improper handling of the solder paste jar will affect the solder paste quality.
- 4) Care must be exercised when applying RMA flux to ensure no excess flux is added to the solar cell. This would cause the solar cell to stick to the ceramic tile during reflow soldering.

## REFERENCES

- Advanced Energy, 2010. *Understanding Potential Induced Degradation*. [pdf] Brinson Blvd Bend, USA: Advanced Energy Industries. Available at: <[http://solarenergy.advancedenergy.com/upload/File/White\\_Papers/ENG-PID-270-01%20web.pdf](http://solarenergy.advancedenergy.com/upload/File/White_Papers/ENG-PID-270-01%20web.pdf)> [Accessed 11 August 2014].
- Amagai, M., 2008. A study of nanoparticles in Sn–Ag based lead free solders. *Microelectronics Reliability*, 48(1), pp.1-16.
- Ami.ac.uk, 2014. *Viscosity and flow*. [online] Available at: <[http://www.ami.ac.uk/courses/topics/0208\\_vaf/index.html](http://www.ami.ac.uk/courses/topics/0208_vaf/index.html)> [Accessed 10 August 2014].
- Anadigics, 2001. *Application Note Solder Reflow Report*. [pdf] Warren, New Jersey, USA: ANADIGICS, Inc. Available at: <[http://www.anadigics.com/site/default/files/application\\_notes/SolderReflowReport.pdf](http://www.anadigics.com/site/default/files/application_notes/SolderReflowReport.pdf)> [Accessed 19 July 2014].
- Calabrese, G., Gualdi, F., Baricordi, S., Bernardoni, P., Guidi, V., Pozzetti, L. and Vincenzi, D., 2014. Numerical simulation of the temperature distortions in InGaP/GaAs/Ge solar cells working under high concentrating conditions due to voids presence in the solder joint. *Solar Energy*, 103, pp.1-11.
- Crandall, M.A., 2011. *Effect of intermetallic growth on durability of high temperature solders (SnAg, SAC305, SAC+Mn, SnAg+Cu Nano) in thermal and vibration environments*. Master. University of Maryland.
- Cuevas, A., 2005. The Early History of Bi-facial Solar Cells. *Bi-facial Solar Cells*. [online] Available at: < [http://www.researchgate.net/publication/251333222\\_THE\\_EARLY\\_HISTORY\\_OF\\_BIFACIAL\\_SOLAR\\_CELLS](http://www.researchgate.net/publication/251333222_THE_EARLY_HISTORY_OF_BIFACIAL_SOLAR_CELLS) > [Accessed 10 August 2014].
- Duran, C., 2012. *Bi-facial Solar Cells: High Efficiency Design, Characterization, Modules and Applications*. Doctor. University of Konstanz.
- Emery, K. & Osterwald, C. R., 1986. Solar Cell. *Solar Cell Efficiency Measurements*, 18(3-4), pp. 253-274.

- Gao, L., Xue, S., Zhang, L., Sheng, Z., Ji, F., Dai, W., Yu, S. and Zeng, G., 2010. Effect of alloying elements on properties and microstructures of SnAgCu solders. *Microelectronic Engineering*, 87(11), pp.2025-2034.
- Hersch, P. and Zweibal, K., 1982. *Basic Photovoltaic Principles and Methods*. [e-book] Cole Blvd Colorado, USA: U.S. Department of Energy. Available at: <<http://www.nrel.gov/docs/legosti/old/1448.pdf>> [Accessed 10 August 2014].
- Hotspot Solar, 2012. *Hotspot Solar*. [online] Available at: <<http://www.hotspotsolar.co.uk/solar/pv/>> [Accessed 5 August 2014].
- Hsieh, H., Lin, F., Yeh, F. and Lin, M., 2009. The effects of temperature and solders on the wettability between ribbon and solar cell. *Solar Energy Materials and Solar Cells*, 93(6), pp.864--868.
- Kim, T. and Kim, Y., 2004. Sn-Ag-Cu and Sn-Cu solders: Interfacial reactions with platinum. *JOM*, 56(6), pp.45-49.
- Lin, L., Song, J., Lai, Y., Chiu, Y., Lee, N. and Uan, J., 2009. Alloying modification of Sn-Ag-Cu solders by manganese and titanium. *Microelectronics Reliability*, 49(3), pp.235-241.
- Lo, C., Lim, Y., Wong, M. and Tian, Y., 2014. The Application of Novel Platinum-Reinforced Tin-Silver-Copper Solder to Bi-facial Photovoltaic Module for Improvement of Yield and Reliability. *J. Sol. Energy Eng.*, 136(4), p.041001.
- Luvata., 2010. *Electrical and Electronic*. [online] Available at: <<http://www.luvata.com/en/About-Luvata/eng-translation/Products/Special-Products/Wire/Electrical-and-Electronic/>> [Accessed 11 August 2014].
- Ostuka, H., M. Sakamoto, K. & Yawaza, Y., 2000. *Progress in Photovoltaics* 8. 8th ed. Lausanne: John Wiley & Sons, Ltd.
- Pingel, S., Frank, O., Winkler, S., Berghold, J., Daryan, S., Geipel, T., Hoehne, H., 2009. Potential Induced Degradation of Solar Cells And Panels. *PID*. [online] Available at: <[http://www.solon.com/export/sites/default/solonse.com/\\_downloads/global/article-pid/Pingel\\_et\\_al\\_PID.pdf](http://www.solon.com/export/sites/default/solonse.com/_downloads/global/article-pid/Pingel_et_al_PID.pdf)>
- Pveducation.org, 2014. *Degradation and Failure Modes*. [online] Available at: <<http://www.pveducation.org/pvcdrom/modules/degradation-and-failure-modes>> [Accessed 24 August 2014].
- RedRing Solder, 2013. *G-series Solder Paste*. [online] Available at: <[http://www.redringsolder.com/solder\\_paste.html](http://www.redringsolder.com/solder_paste.html)> [Accessed 15 August 2014].

- Renewable Energy Policy Network for 21st Century, 2013. *Renewables 2013 Global Status Report*. [pdf] Paris, France: REN21. Available at: <[http://www.ren21.net/Portals/0/documents/Resources/GSR/2013/GSR2013\\_lowres.pdf](http://www.ren21.net/Portals/0/documents/Resources/GSR/2013/GSR2013_lowres.pdf)> [Accessed 3 August 2014].
- Schmid, J. & Schmidt, H. 2011. Power Conditioning for Photovoltaic Power System. In: S. Hegedus & A. Luque, eds. *Handbook of Photovoltaic Science and Engineering*. Chichester: John Wiley & Son Ltd, p.41.
- Schmitt, P., Eberlein, D., Voos, P., Tranitz, M. and Wirth, H., 2011. Metallographic Preparation of Solar Cell Samples for Quality Assurance and Material Evaluation. *Energy Procedia*, 8, pp.402-408.
- Schmitt, P., Kaiser, P., Savio, C., Tranitz, M. and Eitner, U., 2012. Intermetallic Phase Growth and Reliability of Sn-Ag-Soldered Solar Cell Joints. *Energy Procedia*, 27, pp.664-669.
- Shi, Y., Tian, J., Hao, H., Xia, Z., Lei, Y. and Guo, F., 2008. Effects of small amount addition of rare earth Er on microstructure and property of SnAgCu solder. *Journal of Alloys and Compounds*, 453(1-2), pp.180-184.
- Solarserver, 2010. *Basic Knowledge Photovoltaics - SolarServer*. [online] Available at: <<http://www.solarserver.com/knowledge/basicknowledge/photovoltaics.html>> [Accessed 24 July 2014].
- Trowbridge, 2013. *Monocrystalline or Polycrystalline Solar Panels?*. [online] Available at: <[http://www.contemporaryenergy.co.uk/PDF/Article06\\_Mono\\_vs\\_Poly.pdf](http://www.contemporaryenergy.co.uk/PDF/Article06_Mono_vs_Poly.pdf)> [Accessed 3 August 2014].
- Us, A. and Maehlum, M., 2012. *Which Solar Panel Type is Best? Mono-, Polycrystalline or Thin Film?*. [online] Energy Informative. Available at: <<http://energyinformative.org/best-solar-panel-monocrystalline-polycrystalline-thin-film/#thin-film-solar-cells>> [Accessed 24 August 2014].
- Wang, S. and Liu, C., 2007. Coupling effect in Pt/Sn/Cu sandwich solder joint structures. *Acta materialia*, 55(10), pp.3327--3335.
- Wang, Y., Lin, Y. and Kao, C., 2009. Kirkendall voids formation in the reaction between Ni-doped SnAg lead-free solders and different Cu substrates. *Microelectronics Reliability*, 49(3), pp.248-252.
- William, D. and David, G., 2010. *Materials Science and Engineering: An Introduction*. 8th ed. John Wiley.

## APPENDICES

### APPENDIX A: Resistivity Test Data

The resistivity test was carried out for samples which have been heat treated for 1, 3, 5, 12, 24, 48 hours respectively for the solar cells with and without Pt in the solder paste. The voltage for each point on the solar cell was measured and resistance was calculated and tabulated in the tables below.

#### **For Solar Cells without Pt Reinforcement**

**Table of Resistance Value for Each Point on the Bi-facial Solar Cell (Heat Treatment of 1 Hour)**

Point	Current (mA)	Voltage (mV)	Resistance ( $\Omega$ )
1	98.9	0.251	0.00254
2	98.9	0.528	0.00534
3	98.9	0.825	0.00834
4	98.9	1.169	0.01182
5	98.9	1.310	0.01325
6	98.9	1.606	0.01624
7	98.9	1.800	0.0182
8	98.9	2.121	0.02145
9	99.0	2.311	0.02334
10	99.0	2.580	0.02606
11	99.0	2.910	0.02939
12	99.0	3.101	0.03132

**Table of Resistance Value for Each Point on the Bi-facial Solar Cell (Heat Treatment of 3 Hours)**

Point	Current (mA)	Voltage (mV)	Resistance ( $\Omega$ )
1	99.3	0.260	0.00262
2	99.3	0.550	0.00554
3	99.3	0.875	0.00881
4	99.3	1.175	0.01183
5	99.3	1.352	0.01362
6	99.3	1.619	0.01630
7	99.3	1.865	0.01878
8	99.3	2.203	0.02219
9	99.2	2.378	0.02397
10	99.2	2.618	0.02639
11	99.2	3.020	0.03044
12	99.2	3.111	0.03136

**Table of Resistance Value for Each Point on the Bi-facial Solar Cell (Heat Treatment of 5 Hours)**

Point	Current (mA)	Voltage (mV)	Resistance ( $\Omega$ )
1	99.0	0.279	0.00282
2	99.0	0.610	0.00616
3	99.0	0.889	0.00898
4	99.0	1.211	0.01223
5	99.0	1.384	0.01398
6	99.0	1.666	0.01683
7	99.0	1.906	0.01925
8	99.0	2.236	0.02259
9	99.0	2.398	0.02422
10	99.0	2.645	0.02672
11	99.0	3.110	0.03141
12	99.0	3.152	0.03184

**Table of Resistance Value for Each Point on the Bi-facial Solar Cell (Heat Treatment of 12 Hours)**

Point	Current (mA)	Voltage (mV)	Resistance ( $\Omega$ )
1	99.1	0.311	0.00314
2	99.1	0.669	0.00675
3	99.1	0.912	0.00920
4	99.1	1.265	0.01276
5	99.1	1.410	0.01423
6	99.1	1.703	0.01718
7	99.1	1.965	0.01983
8	99.1	2.267	0.02288
9	99.1	2.411	0.02433
10	99.0	2.691	0.02718
11	99.0	3.090	0.03121
12	99.0	3.213	0.03245

**Table of Resistance Value for Each Point on the Bi-facial Solar Cell (Heat Treatment of 24 Hours)**

Point	Current (mA)	Voltage (mV)	Resistance ( $\Omega$ )
1	89.8	0.348	0.00388
2	89.8	0.702	0.00782
3	89.8	1.051	0.01170
4	89.8	1.311	0.01460
5	89.8	1.451	0.01616
6	89.8	1.711	0.01905
7	89.8	1.989	0.02215
8	89.8	2.313	0.02576
9	89.8	2.467	0.02747
10	89.9	2.712	0.03017
11	89.9	3.210	0.03571
12	89.9	3.323	0.03696

**Table of Resistance Value for Each Point on the Bi-facial Solar Cell (Heat Treatment of 48 Hours)**

Point	Current (mA)	Voltage (mV)	Resistance ( $\Omega$ )
1	88.9	0.373	0.00420
2	88.9	0.747	0.00840
3	88.9	1.113	0.01252
4	88.9	1.389	0.01562
5	88.9	1.486	0.01672
6	88.9	1.751	0.01970
7	88.9	2.126	0.02391
8	88.9	2.389	0.02687
9	88.9	2.512	0.02826
10	88.9	2.756	0.03100
11	89.0	3.280	0.03685
12	89.0	3.459	0.03887

**For Solar Cells with 0.40 wt.% of Pt Reinforcement**

**Table of Resistance Value for Each Point on the Bi-facial Solar Cell (Heat Treatment of 1 Hour)**

Point	Current (mA)	Voltage (mV)	Resistance ( $\Omega$ )
1	98.5	0.211	0.00214
2	98.5	0.437	0.00444
3	98.5	0.671	0.00681
4	98.5	0.936	0.00950
5	98.5	1.193	0.01211
6	98.5	1.361	0.01382
7	98.4	1.611	0.01637
8	98.4	1.976	0.02008
9	98.4	2.133	0.02168
10	98.4	2.326	0.02364
11	98.4	2.536	0.02577

12	98.4	2.881	0.02928
----	------	-------	---------

**Table of Resistance Value for Each Point on the Bi-facial Solar Cell (Heat Treatment of 3 Hours)**

Point	Current (mA)	Voltage (mV)	Resistance ( $\Omega$ )
1	99.0	0.218	0.0022
2	99.0	0.444	0.0045
3	99.0	0.681	0.0069
4	99.0	0.945	0.0095
5	99.0	1.209	0.0122
6	99.0	1.378	0.0139
7	99.0	1.629	0.0165
8	99.0	1.989	0.0201
9	98.9	2.154	0.0218
10	98.9	2.348	0.0237
11	98.9	2.553	0.0258
12	98.9	2.931	0.0296

**Table of Resistance Value for Each Point on the Bi-facial Solar Cell (Heat Treatment of 5 Hours)**

Point	Current (mA)	Voltage (mV)	Resistance ( $\Omega$ )
1	98.8	0.238	0.00241
2	98.8	0.457	0.00463
3	98.8	0.723	0.00732
4	98.8	0.959	0.00971
5	98.8	1.219	0.01234
6	98.8	1.379	0.01396
7	98.8	1.654	0.01674
8	98.8	2.012	0.02036
9	98.9	2.167	0.02191
10	98.9	2.356	0.02382

11	98.9	2.573	0.02602
12	98.9	2.963	0.02996

**Table of Resistance Value for Each Point on the Bi-facial Solar Cell (Heat Treatment of 12 Hours)**

Point	Current (mA)	Voltage (mV)	Resistance ( $\Omega$ )
1	98.7	0.236	0.00239
2	98.7	0.476	0.00482
3	98.7	0.758	0.00768
4	98.7	0.975	0.00988
5	98.7	1.233	0.01249
6	98.7	1.371	0.01389
7	98.7	1.679	0.01701
8	98.7	2.03	0.02057
9	98.8	2.179	0.02205
10	98.8	2.374	0.02403
11	98.8	2.622	0.02654
12	98.8	2.989	0.03025

**Table of Resistance Value for Each Point on the Bi-facial Solar Cell (Heat Treatment of 24 Hours)**

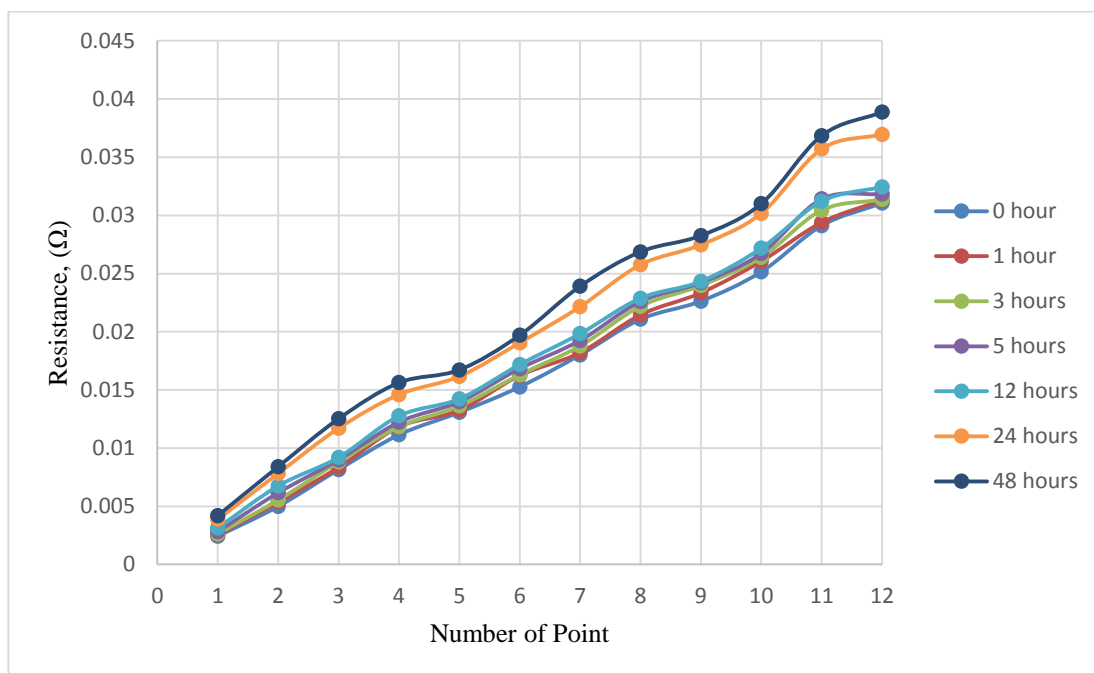
Point	Current (mA)	Voltage (mV)	Resistance ( $\Omega$ )
1	94	0.257	0.00273
2	94	0.500	0.00532
3	94	0.782	0.00832
4	94	1.009	0.01073
5	94	1.265	0.01346
6	94	1.405	0.01495
7	94	1.706	0.01815
8	94	2.056	0.02187
9	94	2.201	0.02341

10	93.9	2.412	0.02569
11	93.9	2.692	0.02867
12	93.9	3.112	0.03314

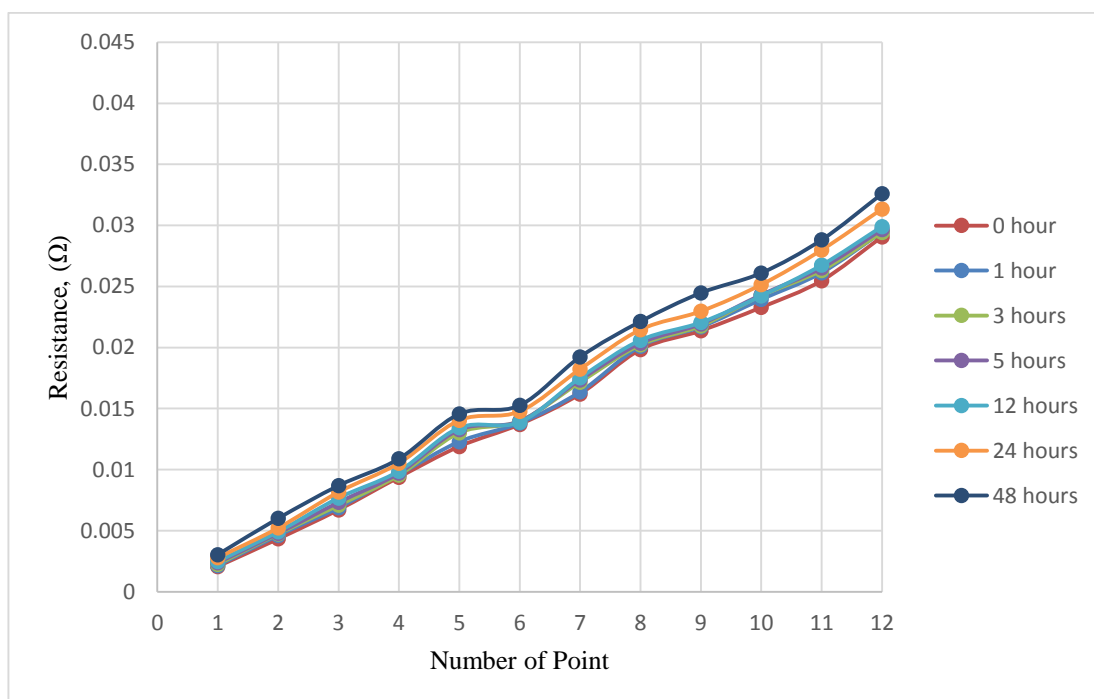
**Table of Resistance Value for Each Point on the Bi-facial Solar Cell (Heat Treatment of 48 Hours)**

Point	Current (mA)	Voltage (mV)	Resistance ( $\Omega$ )
1	94	0.285	0.00303
2	94	0.544	0.00579
3	94	0.81	0.00862
4	94	1.023	0.01088
5	94	1.295	0.01378
6	94	1.433	0.01524
7	94	1.756	0.01868
8	94	2.078	0.02211
9	94	2.268	0.02413
10	93.9	2.456	0.02616
11	93.9	2.712	0.02888
12	93.9	3.221	0.03430

The graph of resistance against the point of solar cell is plotted and shown below.



**Resistance against Points of Solar Cell after Different Periods of Heat Treatment for Solder without Pt**



**Graph of Resistance against Points of Solar Cell after Different Period of Heat Treatment for Solder with 0.40 wt.% of Pt**